Multi-Modal Tsunami Evacuation Planning Considering Evacuees' Non-Compliance Behavior: Istanbul Case Study

Shiva Moslemi[1], Vedat Bayram[2,3], Barış Yıldız[1]

[1]Department of Industrial Engineering, Koç University, Istanbul, Turkey

[2]Department of Analytics, Operations and Systems, Kent University, United Kingdom

[3]Department of Industrial Engineering, TED University, Ankara, Turkey

Abstract

Tsunamis, primarily triggered by earthquakes, pose critical threats to coastal populations due to their rapid onset and limited evacuation time. Two main protective actions exist: sheltering in place, which requires substantial retrofitting investments, and evacuation, which is often hindered by congestion, mixed travel modes, and tight inundation times. Given pedestrians' slower movement and restricted evacuation opportunities, vertical shelters within inundation zones provide essential refuge, while distant horizontal shelters outside these areas are often perceived as safer. As both shelter types complement each other, they must be jointly planned. Evacuation effectiveness is further complicated by noncompliance behavior, which, if neglected, can lead to inefficient retrofitting, capacity overload, and even failure of evacuation strategies. This study introduces a time-expanded multimodal evacuation optimization model that integrates shelter-in-place retrofitting, vertical shelter location, shelter assignment, and routing under tight inundation time, arc and shelter capacities, and compliance likelihoods derived from a survey. The objective is to minimize the time-dependent risk faced by evacuees at home, en route, and at shelters while addressing unsatisfied demand. The model is solved through an integrated Benders Decomposition–Column Generation framework, where Column Generation generates evacuation routes for compliant evacuees and shortest-time paths for noncompliant ones. Convergence is enhanced through decomposition for parallel processing, network simplification, Maximum Density Cuts, and warm-start strategies. The model is applied to Büyükçekmece, a densely populated and highly vulnerable district of Istanbul. Computational results highlight the necessity of incorporating compliance behavior, retrofitting, and vertical shelters into evacuation planning, leading to substantial reductions in overall risk and significant improvements in life safety and evacuation efficiency.

Keywords: Mixed-Mode Tsunami Evacuation; Shelter-in-Place; Vertical Shelter Location; Non-Compliance Behavior; Benders Decomposition; Column Generation

1 Introduction

Disasters have devastating consequences that extend beyond immediate casualties. In addition to the loss of human life, they cause large-scale destruction of infrastructure, disrupt economies,

displace communities, and lead to long-term environmental degradation. With increasing urbanization, climate change, and population growth, both the frequency and severity of disasters have risen, amplifying their impact and making disaster preparedness and response more critical than ever (EM-DAT, 2020a,b).

Among disasters, tsunamis are particularly destructive due to their sudden onset and immense force. Unlike other disasters that develop gradually, tsunamis occur with extremely short lead times, providing little time for evacuation and preparedness. These massive waves, primarily triggered by undersea seismic activity, travel at speeds exceeding 800 km/h in open water and can reach coastal areas within minutes. Upon landfall, they can surge up to 30 meters high, overwhelming communities, destroying infrastructure, and causing severe secondary damage through flooding and debris impact. Some of the most catastrophic tsunami events in history include the 2004 Indian Ocean Tsunami and the 2011 Tohoku Earthquake and Tsunami. The 2004 tsunami, one of the deadliest on record, resulted in nearly 230,000 fatalities across multiple countries. The 2011 tsunami caused over 16,000 deaths, destroyed more than 400,000 homes, and displaced hundreds of thousands of people along Japan's coastline (Maly and Suppasri, 2020). These devastating events highlight the urgent need for effective disaster preparedness and response strategies to mitigate future risks.

Evacuation is one of the most frequently implemented strategies for reducing tsunami-related fatalities. It has been carried out in numerous disasters and has consistently proven effective in saving lives (FEMA, 2019; Bayram, 2016). Reports from the U.S. Department of Homeland Security (DHS), the Federal Highway Administration (FHWA), and the Federal Emergency Management Agency (FEMA) indicate that between 45 and 75 disasters require evacuations annually, often involving thousands of people (FHWA, 2007). However, large-scale evacuations present significant logistical challenges. In densely populated urban areas, limited road capacity and high traffic demand can cause severe congestion, delaying movement and increasing risks for evacuees due to the short available time.

As the scale of evacuation increases, balancing evacuation demand—the number of evacuees or vehicles requiring relocation—and evacuation supply, which refers to the transportation network's capacity to accommodate evacuees, becomes increasingly critical. Poor demand management can lead to congestion on critical routes, while inadequate supply can create bottlenecks that prevent people from reaching safety in time. Therefore, integrating supply and demand management strategies into tsunami evacuation planning is essential to improving evacuation efficiency, reducing congestion, and ultimately minimizing casualties (Bayram and Yaman, 2024). Integrating supply and demand management strategies in tsunami evacuation planning enhances efficiency by optimizing the movement of at-risk populations and improving the overall effectiveness of evacuation plans. Among the most effective supply management strategies is the construction of vertical shelters in addition to existing horizontal shelters. According to the U.S. National Tsunami Hazard Mitigation Program, vertical evacuation involves relocating people to high-rise structures specifically designed to withstand earthquakes and tsunami forces within or very close to high-risk areas. Whereas horizontal evacuation involves moving people to designated shelters outside the inundation zone, typically at higher elevations. In areas with limited road infrastructure and high population density, where evacuation routes are constrained and warning times are extremely short, vertical shelters serve as a necessary complement to horizontal evacuation. While their capacities are limited, they provide immediate protection within inundation zones, especially for pedestrians who cannot reach horizontal shelters in time. Moreover, some evacuees may perceive horizontal shelters outside the inundation area as safer, underscoring the complementary role of both strategies. A key consideration in implementing vertical evacuation includes determining the optimal shelter locations, assess-

ing capacity, and ensuring that the structures meet engineering standards to withstand tsunami impacts. Some reports, including those prepared by the National Oceanic and Atmospheric Administration (NOAA) and the Federal Emergency Management Agency (FEMA), outline the essential requirements for vertical evacuation shelters, emphasizing the need for structurally resilient buildings that can serve as safe havens during tsunamis.

In addition to supply-side measures, demand-side strategies are also effective in tsunami evacuation planning. One widely used approach is sheltering-in-place, in which evacuees remain within retrofitted buildings instead of attempting to evacuate to designated shelters. This strategy reduces both traffic congestion and the risks associated with large-scale movement, and in some regions it represents the only feasible alternative, as residents lack access to any shelter within the available time. However, it is economically impractical to implement on a large scale due to the significant investment and resources required for structural reinforcements. Therefore, a balance must be established between evacuation and shelter-in-place strategies to ensure the most effective allocation of resources while maximizing evacuee safety. Depending on the type and impact of the disaster, the available lead time, the level of protection, the distance from the threat, the duration of exposure, and the degree of road congestion caused by evacuation demand, the decision to evacuate or to shelter in place within a zone may differ (Lindell et al., 2018).

In addition to strategies for managing evacuation demand and supply, several key considerations influence the effectiveness of tsunami evacuation planning, introducing complexities that must be addressed to develop a realistic and efficient evacuation model. One of the major challenges in tsunami evacuation planning is the transportation mode chosen by evacuees, which plays a critical role in determining evacuation performance. Studies indicate that the most effective evacuation mode in tsunamis is on foot, as pedestrian evacuation minimizes congestion, ensures accessibility in dense urban areas, and eliminates reliance on road networks that may be damaged or overwhelmed (Scheer et al., 2011). However, vehicular evacuation may still be feasible in areas with low population density, sufficient road infrastructure, and early tsunami warnings. Most studies in the literature consider only pedestrian or only vehicle-based evacuations, failing to account for mixed evacuation scenarios where both modes coexist. To better reflect real-world conditions, mixed pedestrian–vehicle evacuation should be analyzed.

Another critical factor influencing tsunami evacuation planning is noncompliance behavior, which can significantly disrupt evacuation efforts. Noncompliance may arise due to personal safety concerns, distrust in authorities, or prior disaster experiences, but its extent varies depending on individual decision-making. In evacuation decisions, individuals may disregard official evacuation orders due to socio-demographic factors (such as residence duration, income level, family composition, and pet ownership) and risk perception (Gladwin and Peacock, 1997; Solís et al., 2010; Whitehead et al., 2000). Additionally, concerns about traffic congestion and evacuation delays can deter people from leaving, as seen during Hurricane Floyd, where 65% of non-evacuees cited anticipated traffic congestion as their primary reason for staying behind (Dow and Cutter, 2000). Similarly, in shelter-in-place decisions, individuals may choose to remain in their homes if they perceive their structures to be strong enough to withstand the disaster, while others may be forced to stay due to mobility limitations, medical needs, or lack of access to evacuation resources (Whitehead et al., 2000; Sorensen et al., 2004). The complexity of evacuation planning is further exacerbated when evacuees act selfishly, relying on familiarity and routine by choosing the shortest or most familiar routes rather than designated safer alternatives, which contributes to severe congestion and delays (Lindell et al., 2011; Wu et al., 2012). For instance, during Hurricane Bret, 69% of evacuees selected their routes based on past experience rather than following official guidance, exacerbating congestion and reducing

overall evacuation efficiency (Prater et al., 2000). Therefore, in tsunami scenarios, noncompliance can lead to severe congestion and unexpected bottlenecks, increasing risks for evacuees and disrupting planned evacuation routes. Evacuation models must incorporate noncompliance behavior to develop more realistic and effective evacuation strategies that account for the complexities of human decision-making during disasters.

Based on these challenges, this research aims to address the following research questions:

1. Which zones' buildings should be retrofitted, how many residents in these retrofitted buildings are likely to remain at home, and what level of risk is associated with sheltering in place?

2. What are the expected evacuation demands of each zone across different transportation modes?

3. Where should vertical shelters be constructed given capacity and budget constraints, and what is the level of risk for evacuees staying in each vertical shelter?

4. To which shelters should pedestrians from each zone be allocated, considering travel risks and the available capacity of vertical shelters?

5. Which routes should be used for evacuating people by vehicle, taking into account risks, road segment capacities, and available lead time, and to what extent will drivers comply with these route assignments?

To address the research questions, this study develops a model on a time-expanded network to ensure safe vertical and horizontal evacuation of mixed pedestrians and vehicles under tsunami threat. The model incorporates the timing of tsunami wave arrivals, evacuees' departure times (staggered by sub-zones rather than departing simultaneously), and constraints imposed by traffic congestion. Unlike most existing models that assume full compliance with official instructions, this study not only considers partial compliance but also incorporates some of the influencing factors of compliance into a unified framework to enhance compliance.

In the developed model, demand-management decisions such as whether to evacuate or shelter in place, shelter assignment (horizontal or vertical), and routing are optimized. On the supply-management side, vertical shelter location decisions are also treated as decision variables. These decisions must be made with respect to the risks and hazards posed by the disaster. Time-based performance measures, such as the clearance time of the last evacuee or total evacuation time, may not necessarily correspond to the safest options. Therefore, the model incorporates spatial-temporal risk assessment, aiming to minimize evacuees' time-dependent exposure to tsunami impacts. The objective is to reduce cumulative risk for those remaining at home, traveling on evacuation routes, and located in shelters by assigning evacuees to paths that remain safe longer considering inundation time, and by maximizing the number who reach safety through imposing a large penalty on unmet demand.

To solve the problem effectively for realistic instances, an exact solution methodology based on Benders decomposition is proposed. Within this framework, column generation is employed to identify feasible evacuation routes, focusing computational effort only on the most promising routes. To overcome the slow convergence often encountered in Benders decomposition, several acceleration strategies are incorporated: (i) decomposing the subproblems for vehicles and pedestrians to enable parallel processing, (ii) reducing network size by eliminating redundant nodes, arcs, and routes, (iii) employing warm-start strategies in which initial solutions transfer relevant subproblem information to the master problem to enhance convergence, (iv) applying

the Maximum Density Cut (MDC) method to generate high-density cuts that encompass large sets of decision variables, and (v) using callback mechanisms in branch-and-cut algorithms. For column generation, initial solutions are also introduced to accelerate the identification of promising routes.

The need for effective tsunami evacuation planning in Istanbul is underscored by recent studies and official action plans. According to the Istanbul Province Tsunami Action Plan prepared by the Istanbul Metropolitan Municipality (İBB) and the Middle East Technical University (ODTÜ) (İBB-ODTÜ, 2019), the expected Istanbul earthquake could trigger secondary tsunami hazards, severely affecting districts along the shores of the Marmara Sea. This concern is further emphasized in the report of the Earthquake Investigation Commission of the Grand National Assembly of Turkey (TBMM, 2021). Modeling studies for the Marmara Sea suggest that the first tsunami waves could reach the shoreline within 10 minutes of the earthquake, while the maximum waves could arrive within 60–90 minutes, particularly threatening Eastern Marmara, including the Princes' Islands (İBB-ODTÜ, 2018, 2019; Necmioglu et al., 2018). These studies estimated inundation areas, wave heights, building vulnerability, and evacuation-route serviceability. Simulation-based risk assessments conducted jointly by İBB and ODTÜ identified Büyükçekmece as one of the most vulnerable districts, with extensive inundation zones, high flow depths, and a large resident population. Accordingly, this study adopts Büyükçekmece as the case study to evaluate tsunami evacuation planning against the potential threat of a secondary tsunami following the anticipated Istanbul earthquake.

The rest of the paper is organized as follows: Section 2 presents a thorough review of the literature and outlines the contributions. Section 3 describes the problem setting and assumptions and introduces a mathematical formulation for the model. Section 4 proposes an integrated Benders–Column Generation solution method and the suggested acceleration strategies. Section 5 reports results under different assumptions, sensitivity analyses on critical parameters, the effects of acceleration methods, and managerial insights derived from real data on the case study. Section 6 concludes the paper and highlights future research directions.

2 Literature Review

To provide a comprehensive foundation for this study, this section reviews key literature on tsunami evacuation planning, focusing on three critical aspects: shelter-in-place strategy, Tsunami vertical shelter location models, and compliance behavior. The first part examines studies that consider shelter-in-place as a protective decision, highlighting conditions under which staying at home—whether supported by retrofitting or not—can be a feasible and effective alternative to evacuation across different disasters. The second part explores approaches for determining optimal locations of Tsunami vertical shelters, emphasizing accessibility and safety. Finally, the third part discusses how compliance and behavioral variability have been incorporated into evacuation optimization models, and how determinants of compliance—such as socio-demographic, psychological, and situational factors—are modeled to improve realism and effectiveness.

2.1 Shelter-in-place decisions in evacuation optimization

The decision to evacuate or shelter in place is among the most critical in emergency management, requiring a careful balance between potential health risks and protective benefits. Evacuation involves relocating people from the threat area to horizontal shelters outside the danger

zone or to vertical shelters within it that offer sufficient protection, whereas shelter-in-place refers to remaining at home when evacuation is unsafe or impractical, relying on the dwelling's inherent protection (Cova et al., 2011). The choice between these strategies depends on several interrelated factors, including the nature and intensity of the hazard, the protective capacity of shelters (e.g., fire-resistant homes for wildfires or reinforced tall buildings for tsunamis), available warning and travel times, route and destination conditions, and the vulnerability or mobility of the population (Cova et al., 2011; Lindell and Perry, 2012; Sorensen et al., 2004). Although evacuation has been extensively studied through optimization models focusing on routing and shelter allocation, relatively few models explicitly incorporate shelter-in-place as an alternative protective strategy.

Cova et al. (2011) were among the first to address this issue through an optimization model for wildfire management that integrates evacuation, shelter-in-refuge, and shelter-in-home options. The model maximizes community protection by assigning each household to the option offering the highest safety margin—defined as the difference between the level of protection and expected fire threat—while accounting for warning time, travel duration, fire intensity, structural resistance, and congestion effects. Their results indicate that evacuation is preferred when time and routes permit safe movement, whereas limited time or blocked roads make shelter-in-place or refuge shelters more appropriate. Karabuk and Manzour (2019) extended this line of research to tornado response management under uncertainty using a multi-stage stochastic programming model that determines, at each forecast stage, whether residents should evacuate or shelter in place. The model represents evolving tornado paths and intensities through a probabilistic forecast tree and minimizes expected injuries and fatalities based on hazard intensity, location, and the protection level of homes, vehicles, or safe zones. It integrates stage-wise recourse, temporal feasibility, and cell-transmission-based traffic dynamics (CTM) to ensure feasible movement within the available time. Results show that this adaptive approach outperforms static shelter-in-place policies by recommending evacuation only when lead time and safe routing allow. Similarly, Apivatanagul et al. (2012) developed a time-dependent, two-stage stochastic model for hurricane evacuation planning that jointly determines who should evacuate, who should shelter in place, and when to depart, introducing departure-time optimization as a new dimension in decision-making. The model minimizes total societal cost by balancing expected life-safety risk, travel time, and time away from home, while considering road capacity, phased departures, and route connectivity. The results demonstrate that optimizing departure timing alongside evacuation and shelter-in-place decisions improves both network efficiency and overall safety outcomes.

In these models, shelter-in-place strategies were incorporated without considering retrofitting, assuming that existing buildings provide adequate protection. While this assumption may hold for wildfires, it is unrealistic for hazards such as hurricanes, earthquakes, or tsunamis, where structural reinforcement is essential for safety. Hughes et al. (2022) addressed this limitation through a multi-objective optimization framework aimed at improving the resilience of coastal residential communities via two retrofitting strategies—building elevation and construction-quality enhancement—under budget constraints. The model minimizes structural damage, morbidity, displacement, mitigation cost, and total economic loss, assuming a fixed evacuation probability for the community. Although evacuation is not a decision variable, the study highlights that structural improvement is a prerequisite for effective shelter-in-place in high-risk zones. In contrast, Jiang et al. (2022) focused on short-term shelter-in-place decisions that do not require retrofitting. Their Emergency Response Trade-off model for chlorine leakage accidents integrates gas-dispersion simulation, building infiltration dynamics, and evacuation routing to determine the optimal duration of indoor sheltering. The results show that remain-

ing indoors for a limited time effectively reduces exposure and congestion, whereas prolonged sheltering increases indoor contamination. This demonstrates that, unlike other hazards where structural improvement is required, homes can still provide meaningful short-term protection in chemical accidents, serving as temporary refuges before evacuation and highlighting the critical role of timing in minimizing risk.

Recent studies have also explored multi-hazard resilience through optimization-based retrofitting strategies. Braik et al. (2025) proposed a probabilistic optimization framework for coastal retrofitting against wind, storm surge, and flooding, jointly evaluating building elevation and roof reinforcement under budget constraints to minimize cumulative risk and socioeconomic disparity. Although evacuation is not modeled explicitly, their results show how retrofitting enhances in-place protection and reduces displacement and economic disruption during hurricanes. Similarly, Gupta et al. (2024) presented a multi-hazard optimization framework that also considers relocation in addition to retrofitting as complementary pre-disaster strategies against combined earthquake–tsunami hazards. Their multi-objective model, applied to Seaside, Oregon, minimizes economic loss, dislocation, and repair time under budget constraints by evaluating three alternatives: retrofitting to higher seismic standards, relocating buildings from inundation zones, and combining both. Results indicate that seismic retrofitting enables safe shelter-in-place after earthquakes, while relocation is critical for sustaining community stability in tsunami-prone areas. However, conventional seismic retrofitting was assumed ineffective within inundation zones, as it neglects hydrodynamic, debris-impact, and scouring effects. This highlights a remaining research gap—the need for tsunami-specific retrofitting capable of providing both seismic and hydrodynamic protection, consistent with evidence from reinforced buildings that have withstood dual-hazard forces during past events. Despite these advances, a broader research gap remains. Existing optimization models for tsunami evacuation primarily focus on evacuation itself, while one study addresses permanent relocation (i.e., permanent evacuation). More broadly, there is still no integrated framework that jointly considers evacuation decisions and investment in retrofitting to balance safety, feasibility, and resource allocation across disasters.

2.2 Tsunami Vertical Shelter Location

In coastal regions exposed to near-field tsunamis, evacuation time is often too short for residents to reach safe high grounds. In such contexts, vertical evacuation shelters play a vital role by offering immediate refuge within inundation zones. Determining appropriate locations for these structures is a multifaceted challenge that demands balancing physical, social, and logistical considerations. Factors such as population density, network connectivity, walking speed, and available lead time must all be harmonized to ensure timely accessibility. Moreover, in areas with limited early warning systems, spatial risk assessment becomes a crucial component of the planning process.

Researchers have explored a wide range of analytical methods to identify effective locations for vertical shelters. Spatial and simulation-based approaches have been the most common, often employing Geographic Information Systems (Geographic Information System, GIS) to integrate hazard maps with demographic and infrastructural data. For instance, Nakai et al. (2022) and Dewi (2012) applied GIS-based models that considered factors like distance, shelter capacity, and building strength to locate suitable public structures—such as schools, towers, or mosques—for vertical evacuation. Later studies enhanced these frameworks by including community-based priorities. Wood et al. (2014) combined GIS and multi-criteria decision analysis (MCDA) to reflect local perceptions, emphasizing shelter accessibility for vulnera-

ble groups and accounting for features like bridge crossings and hazard proximity. Similarly, simulation-oriented works—such as Mawardin (2018) and Mostafizi et al. (2019)—integrated field surveys, tsunami propagation modeling, and evacuation simulations to evaluate shelter usability, structural reliability, and travel behavior.

While such spatial and simulation models provide valuable insight into evacuation dynamics, they are often limited when it comes to analyzing large-scale alternatives or assessing interactions among multiple shelters. To overcome these limitations, optimization-based approaches have been introduced. Park et al. (2012), for example, formulated a genetic algorithm that selected shelter locations minimizing evacuation time in Cannon Beach, Oregon, showing substantial reductions in expected casualties. Doerner et al. (2009) proposed a multi-objective formulation that jointly considered construction cost, risk level, and distance, offering trade-offs among different shelter categories including elevated structures, retrofitted buildings, and naturally high areas. González-Riancho et al. (2013) further developed an integrated approach combining GIS mapping, evacuation-time estimation, and optimization for shelter allocation. More recently, Sotelo-Salas et al. (2024) incorporated regional assignment constraints, shelter height, and capacity limits to provide a more realistic and operationally feasible framework.

Building upon these contributions, this study extends the literature by developing an optimization-based model that minimizes total tsunami risk through the joint determination of vertical shelter locations and pedestrian assignments across vertical, horizontal, and shelter-in-place (retrofitted) options. Unlike previous studies that examined these strategies separately, the proposed model considers their interdependence and the trade-offs among them under realistic behavioral and physical conditions. It incorporates survey-calibrated walking tolerance, time-dependent risk exposure, limited shelter capacity, departure time, and non-compliance behavior with retrofitted shelters—factors that significantly affect accessibility and safety. By integrating these components within a unified framework, the study provides a balanced and realistic approach to tsunami evacuation planning, supporting decisions that account for both infrastructural constraints and human behavior.

2.3 Incorporating Evacuee Compliance into Optimization Models

Compliance behavior is a critical factor in evacuation planning, as deviations can substantially affect overall system performance. Many studies, including two comprehensive surveys, emphasize the importance of incorporating behavioral considerations into evacuation optimization (Caunhye et al., 2012; Bayram, 2016; Aldahlawi et al., 2024). Nevertheless, most optimization models still adopt simplified assumptions that fail to capture the diversity of real-world responses, thereby limiting both realism and applicability.

Most optimization models addressing compliance behavior focus on routing and rely on idealized, binary assumptions. System-optimal (SO) models represent full compliance, user equilibrium (UE) reflects non-compliance, and constrained system-optimal (CSO) models introduce behavioral realism through fairness constraints but continue to assume evacuees comply fully once these are satisfied. CSO models therefore mark the first progress toward behaviorally aware optimization. However, only a limited number of studies explicitly incorporate partial compliance, evaluating the operational impacts of varying compliance rates within optimization frameworks (Arıkanoğlu et al., 2025). Only a limited number of studies have explicitly incorporated *partial compliance* within optimization frameworks to assess the operational impacts of varying compliance rates.

A prominent contribution in this area is by Lessan and Kim (2022), who investigate compliance with routing decisions in short- and no-notice evacuations such as wildfires. In their

model, evacuees are initially assigned to routes assuming full compliance, while actual behavior is captured through a *diversion matrix* that reallocates flows among alternative paths. In deterministic settings, a fixed diversion matrix is applied; in stochastic settings, multiple matrices are generated from a uniform distribution to reflect uncertainty in compliance. Congestion is modeled using the Bureau of Public Roads (BPR) function:

$$t_{ij}(x_{ij}) = t_{ij}^0 \left(1 + \alpha \left(\frac{x_{ij}}{c_{ij}}\right)^\beta\right) \tag{1}$$

where t_{ij}^0 denotes the free-flow travel time, c_{ij} is the arc capacity, and x_{ij} is the flow on arc (i, j). Under uncertainty, evacuation performance is evaluated with a Conditional Value-at-Risk (CVaR) objective:

$$\text{CVaR}_\theta = \min_\eta \left\{\eta + \frac{1}{M(1-\theta)} \sum_{m=1}^{M} [W(f, \beta_m) - \eta]^+\right\} \tag{2}$$

where $W(f, \beta_m)$ represents evacuation time under diversion matrix β_m. This framework explicitly quantifies the effects of route deviations on congestion and enhances robustness in evacuation planning.

Building on this behavioral perspective, Wang and Wallace (2022) extend compliance modeling to *destination assignment* by proposing a two-stage stochastic optimization model for allocating evacuees to pick-up points. Compliance is treated as scenario-dependent: in each scenario s, a fraction δ_{is} of evacuees from demand point i follow the assigned pick-up point, while the remaining $(1 - \delta_{is})$ choose alternatives. Two noncompliance strategies are introduced—the deterministic BEST rule, where evacuees select the single most attractive alternative, and the probabilistic BETTER rule, where evacuees redistribute among multiple attractive options. The attractiveness of pick-up point j in scenario s is expressed as:

$$\rho_{ijs} = \omega_i \cdot \exp\left(-\iota_i^s \cdot \frac{t_{ij} - \sigma_i}{\sigma_i}\right) + (1 - \omega_i) \cdot \exp\left(-\zeta_i^s \cdot \frac{\theta_i - a_{ij}}{\theta_i}\right) \tag{3}$$

where t_{ij} and a_{ij} are travel time and directional angle; σ_i and θ_i denote the minimum and maximum values for demand point i; ι_i^s and ζ_i^s are scenario-specific sensitivity factors; and $\omega_i \in [0, 1]$ balances the importance of time and direction. Under the BETTER rule, evacuees initially assigned to j' but choosing j follow:

$$\mu_{ijj's} = \begin{cases} \dfrac{\rho_{ijs}}{\sum_{k \in B_{ij's}} \rho_{iks}}, & \text{if } \rho_{ijs} > \rho_{ij's}, \\ 0, & \text{otherwise.} \end{cases} \tag{4}$$

where $B_{ij's}$ represents pick-up points more attractive than j'. This model minimizes a weighted sum of expected overflow and travel time, subject to assignment, capacity, and compliance constraints. Results demonstrate that the BETTER strategy increases robustness by enabling flexible redistribution and reducing both overflow and delay.

Further extending the behavioral dimension, Sun et al. (2017) examine *evacuation participation compliance* in hurricane scenarios. Their dynamic optimization model links participation rates to warnings disseminated through various communication channels. The compliance

of evacuees of type i with a warning from source j at time t is denoted p_{ijt}, which varies by source credibility, timing, and household characteristics. If a warning is issued ($x_{ijkt} = 1$), the number of evacuees complying is given by:

$$x_{ijkt} \cdot p_{ijt} \cdot n_{ikt} \tag{5}$$

where n_{ikt} is the remaining population of that group in zone k at time t. The dynamic population updates introduce nonlinearity, and a greedy heuristic optimizes warnings sequentially over time, effectively capturing evolving compliance and improving participation.

Expanding the scope to *multiple interdependent decisions*, Yi et al. (2017) integrate compliance with route choice, destination selection, and evacuation timing—again within a hurricane context. Routing is represented through dynamic user equilibrium to capture self-routing behavior, while compliance with departure time and destination assignment is modeled using discrete choice. For instance, the probability of evacuation at time t is estimated via a sequential logit model:

$$P^s_{z,t}(\text{evac}) = \frac{\exp(\beta' X^s_{z,t})}{1 + \exp(\beta' X^s_{z,t})} \tag{6}$$

where $X^s_{z,t}$ includes variables such as evacuation orders, proximity to the hurricane, and socio-demographic factors. Destination choice is captured through a nested logit distinguishing between public shelters and exits from the study area. The model is solved with progressive hedging, enabling adaptive planning across scenarios and providing one of the few frameworks that jointly consider compliance across several interdependent evacuation decisions. Some studies have integrated influencing factors such as physical constraints and psychological states directly into optimization models to enhance compliance behavior (Arıkanoğlu et al., 2025).

Physical capabilities, particularly mobility limitations and vulnerability, significantly influence evacuees' compliance behavior. Hsiao et al. (2021)develop two optimization models for local refuge planning during dam-break floods, where evacuation is limited to walking. The models determine whether to open a shelter, which capacity level to select (small, medium, or large), and how to assign evacuees—classified as general public or elderly—to shelters within acceptable walking distances (500 m and 300 m, respectively). The first model maximizes the number of evacuees assigned to shelters by prioritizing vulnerable groups through weights w_k:

$$\max \sum_k \sum_j \sum_i p_i w_k y_{ijk} \tag{7}$$

where y_{ijk} is the proportion of evacuees of class k from node i assigned to shelter j, p_i is the population at node i, and a_{ijk} ensures assignments respect walking limits. The second model incorporates spatial risk by using d_i (the inverse of distance from the river) to prioritize high-risk areas:

$$\max \sum_k \sum_j \sum_i p_i w_k d_i y_{ijk} \tag{8}$$

While the first model favors larger shelters in dense areas to maximize coverage, the second directs resources toward smaller shelters in high-risk zones, improving accessibility and protection for vulnerable groups. By embedding vulnerability weights, spatial risk, and mobility constraints, the framework strengthens both equity and compliance feasibility.

Psychological dynamics have also been incorporated into optimization frameworks. Hu et al. (2014) propose a post-disaster evacuation and resettlement model based on the 2008 Wenchuan earthquake, where evacuees' mental states evolve with environmental stressors. At each time t and site s, individuals are categorized as susceptible ($x^S_{t,s}$), infective ($x^I_{t,s}$), or removed ($x^R_{t,s,d}$). Panic propagation is captured by:

$$x^{NIP}_{t,s} = \beta_{t,s} \cdot x^I_{t,s} \cdot \frac{x^{NIP}_{t,s} + x^S_{t,s}}{x^I_{t,s} + x^{NIP}_{t,s} + x^S_{t,s}} \tag{9}$$

where $\beta_{t,s}$ represents the panic spread strength, influenced by the panic degree α_t and government intervention $g_{t,s}$:

$$g_{t,s} = \sigma \cdot \frac{e_{t,s}}{x^I_{t,s} + x^{NIP}_{t,s} + x^S_{t,s}} \tag{10}$$

with $e_{t,s}$ denoting the number of deployed mental health workers and σ representing the support capacity per worker. The model minimizes the total cost, including psychological, transportation, deployment, and shelter costs, subject to resource and intervention constraints. The results indicate that timely psychological support reduces panic propagation and improves compliance.

Dulebenets et al. (2020) address behavioral and psychological heterogeneity more comprehensively through a multi-objective evacuation planning model that jointly optimizes departure time, route, and shelter assignment. The model minimizes six burdens affecting evacuees: evacuation time, mental demand, physical demand, temporal demand, effort, and frustration. These burdens are aggregated into a single objective weighted by the number of evacuees per vehicle, capturing behavioral variability and discomfort. By integrating human-related attributes—such as age, health condition, experience, and driving ability—into both objectives and constraints, the model provides a human-centered representation of compliance and fairness under stress.

In total, only a limited number of optimization studies have incorporated partial compliance, and those that have typically focus on specific decision types—such as routing, destination assignment, participation, or combined decisions—within disaster contexts like wildfires or hurricanes. Most rely on simplified or synthetic behavioral assumptions rather than empirically grounded data. Moreover, many of these models are disaster-specific; for example, compliance with departure time is relevant for long-notice events such as hurricanes but less meaningful for highly time-constrained disasters like tsunamis. Critical aspects such as compliance with shelter-in-place decisions remain largely unmodeled, and distinctions between transportation modes—such as pedestrians and vehicles—are rarely incorporated. Even models that consider underlying behavioral drivers, including mobility constraints or psychological responses, often follow CSO-like assumptions, presuming full compliance once specific needs are met. Consequently, no existing study fully integrates compliance rates in a way that reflects real-world behavior while accounting for these influencing factors that increase evacuees' compliance levels.

Building on the identified research gaps, the key contributions of this study are summarized as follows:

- A unified optimization is formulated in which vertical-shelter location, the evacuate–versus–shelter-in-place choice, routing, and assignment are decided jointly.
- Shelter-in-place is endogenized for the first time in tsunami evacuation modeling by allowing only hydrodynamically retrofitted or engineered buildings to serve as viable

in-place refuge, thereby enabling safe protection within inundation zones without the need for permanent relocation. The proposed model balances this decision with vertical and horizontal evacuation options to ensure optimal protection across coastal sub-zones within the available warning lead time.

- Partial compliance with shelter in place and routing is incorporated, calibrated from survey data, and compliance-supporting design choices are embedded—such as directional filtering of arcs away from the coastline and proximity-tolerance–based guidance—so that plans both remain effective under partial adherence and actively enhance adherence. Compliance behavior is incorporated separately for pedestrians and vehicles. Compliance behavior is incorporated separately for pedestrians and vehicles (Figure 3).

  For pedestrians, two types of decisions were modeled: shelter-in-place and assignment. In the shelter-in-place case, individuals without access to a horizontal shelter were classified as *mandatory compliant*, as remaining at home was their only option. For those with access, compliance was differentiated between *fully compliant*, who stayed at home as instructed, and *noncompliant*, who evacuated to the nearest horizontal shelter along the shortest path. Compliance rates were derived from survey data. In assignment, pedestrians were directed to shelters within an acceptable tolerance range, for which full compliance was assumed.

  For vehicles, compliance was modeled through shelter-in-place and routing decisions. The shelter-in-place logic followed the same structure as for pedestrians: evacuees without access to a horizontal shelter were mandatory compliant, while others could be fully compliant or noncompliant. In routing, compliance was represented by an S-curve function of the time difference between the suggested and shortest routes. Drivers classified as fully compliant followed the suggested route, whereas noncompliant drivers selected the shortest-time path.

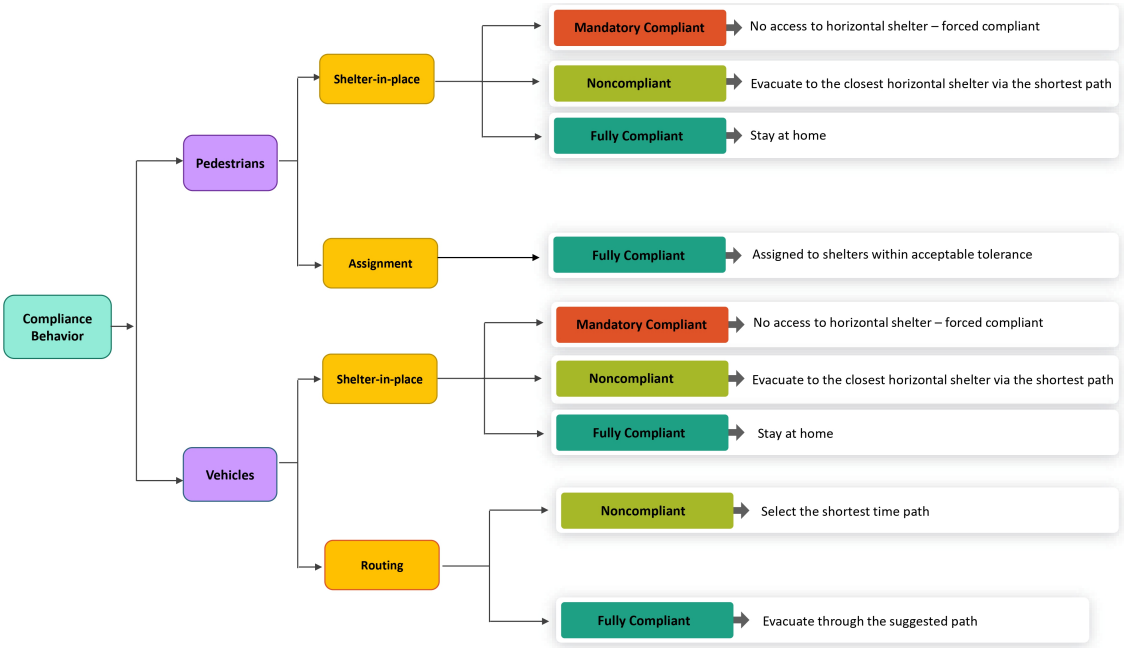

Figure 1: Compliance behavior framework for pedestrians and vehicles.

- Vertical-shelter planning is addressed via an optimization approach: candidate locations are aligned with the Istanbul Tsunami Action Plan, and optimal locations and opening

decisions are selected considering population distribution, accessibility, hazard exposure, and pedestrian proximity tolerance, guided by simulation-derived, time-dependent risk.

- Multi-modal evacuation is modeled on distinct pedestrian and vehicular networks with mode-specific demand, arc eligibility via directional filtering, route and shelter selection criteria, and speeds, with common departure times and timing limits across modes.
- A risk-minimization objective on a time-expanded network is employed: simulation-derived, time-evolving inundation risk is minimized rather than travel time; lead/inundation-time constraints are enforced; traffic congestion is controlled; and unmet demand is heavily penalized—unlike prevailing time-minimization or static-access models.
- The framework is instantiated for Büyükçekmece (Istanbul) using realistic data and inputs derived from surveys and tsunami simulations, incorporating behavioral and operational factors such as compliance rate, departure time, vehicle usage, and walking tolerance..
- A tailored Benders decomposition with column generation is used: two pricing problems generate route sets for compliant and non-compliant flows, and acceleration strategies are applied to obtain optimal solutions within practical runtimes.

3 Problem Definition and Mathematical Formulation

This section describes the tsunami evacuation problem, explains the construction of the time-expanded network together with the underlying assumptions, and presents the mathematical model formulated for the problem.

3.1 Problem Description

The evacuation planning problem is formulated on a directed graph $G(N, A)$, representing a static evacuation network where N is the set of nodes and A is the set of directed arcs. The node set N consists of three subsets: the set of evacuation sub-zones (O), the set of intersection nodes (J), and the set of shelters (S). The shelter set is further divided into candidate locations for vertical shelters (S^v) and designated horizontal shelters (S^h). The arc set A is classified into pedestrian paths (A^p) and shared vehicle–pedestrian roads (A^w). Each evacuation sub-zone $o \in O$ is connected to a shelter $s \in S$ through a set of predefined routes $\Pi_{(o,s)}$, where each route consists of a sequence of arcs A_π.

Once a tsunami warning is issued, real-time monitoring systems provide estimates of the expected arrival time and flow depth of tsunami waves at different locations. The present study focuses on the worst-case scenario. Local authorities disseminate protective action recommendations—either advising residents to shelter in place or to evacuate to designated shelters via specific routes—through various communication channels such as social media, text messages, and mobile alerts.

Evacuees in each sub-zone decide whether to evacuate on foot or by private vehicle. The evacuation demand originating from sub-zone o is denoted by d_o^p and d_o^w for pedestrians and vehicles, respectively.

Figure 2 illustrates a simplified evacuation network composed of five evacuation sub-zones ($o1$–$o5$), four intersection nodes ($j1$–$j4$), three candidate vertical shelters ($v1$–$v3$), and two horizontal shelters ($h1$, $h2$). The numerical value following each node's label indicates the

tsunami wave arrival time in minutes. For instance, $o1, 4$ means that the tsunami waves reach sub-zone $o1$ after four minutes. Arc labels represent travel times for vehicles and pedestrians, respectively. Since pedestrians move more slowly and their speed depends on the terrain slope, their travel times are generally longer.

Among the candidate vertical shelters, only $v1$ and $v3$ are opened under the available budget (B). Additionally, sub-zones $o1$ and $o3$ are retrofitted as part of pre-disaster preparedness. In $o1$, pedestrians cannot reach the nearest horizontal shelter ($h1$) even under ideal conditions with no congestion and immediate departure. The travel time alone exceeds the available window, making retrofitting the only feasible strategy to enhance safety. Moreover, when comparing sub-zones $o2$ and $o3$, retrofitting $o3$ is prioritized because its evacuation demand is higher and nearby shelter capacities are insufficient, leading to greater potential risk. Retrofitting this sub-zone therefore provides a more effective measure to reduce vulnerability and improve overall safety.

In retrofitted sub-zones, authorities instruct residents to shelter in place rather than evacuate. However, compliance with this directive is uncertain. Some evacuees—whether traveling on foot or by vehicle—may distrust the structural integrity of their buildings or the credibility of official guidance, or they may perceive more distant locations as safer. Consequently, a portion of residents may still attempt to evacuate despite instructions to remain indoors. Understanding these behavioral responses is essential for designing effective and realistic evacuation plans.

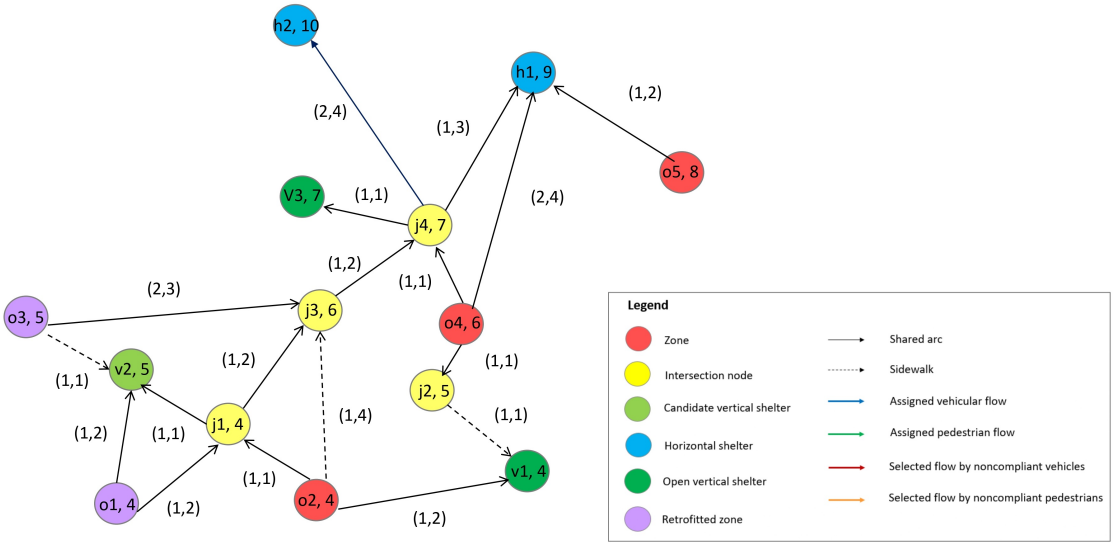

Figure 2: Sample evacuation network

Figures 3a and 3c illustrate the behavioral responses of pedestrians and drivers in retrofitted sub-zones to official shelter-in-place (SIP) recommendations. Pedestrian behavior is depicted in Figure 3a. When the SIP strategy is implemented in a sub-zone o, a proportion of residents—denoted by $(1 - \sigma_o^p)$—distrust the structural resistance of their buildings and choose to evacuate instead of remaining indoors. These noncompliant pedestrians prefer to move toward the nearest horizontal shelter following the shortest available route. For instance, in sub-zone $o3$, a fraction σ_{o3}^p of pedestrians comply with the SIP directive and stay at home, while the remaining $(1-\sigma_{o3}^p)$ noncompliant individuals attempt to reach shelter $h1$. In contrast, in sub-zone $o1$, the nearest horizontal shelter ($h1$) is located beyond the safe travel distance, meaning that pedestrians cannot reach it before the inundation time regardless of their departure time or arc capacity. Therefore, it is assumed that all pedestrians in $o1$ fully comply with the SIP directive,

i.e., $\sigma^p_{o1} = 1$.

Vehicle behavior under the same conditions is shown in Figure 3c. Considering both departure times and traffic congestion, noncompliant drivers in sub-zone $o1$ can still reach the nearest horizontal shelter ($h1$), indicating partial noncompliance. However, among the noncompliant vehicles originating from sub-zone $o3$, only a portion can reach $h1$ before inundation, while the remaining vehicles fail to arrive due to limited arc capacities and are therefore assumed to be lost during evacuation.

For non-retrofitted sub-zones, authorities must assign evacuees—whether pedestrians or vehicle users—to horizontal or open vertical shelters based on tsunami risk, available time (derived from inundation and departure times, as sub-zones may not depart simultaneously), and the capacity of shelters and arcs. Vehicles in each sub-zone can be routed to multiple horizontal shelters through different paths, but they are only allowed to use vehicular arcs. In contrast, pedestrians from each sub-zone o are assigned to only one vertical or horizontal shelter located within an acceptable tolerance degree (ε). The acceptable tolerance degree corresponds to shelters whose path lengths are less than or equal to $(1+\varepsilon)$ times the length of the route to the nearest shelter; routes longer than this threshold are excluded from consideration. Pedestrians travel through the closest sidewalks or shared arcs, and it is assumed that both vehicles and pedestrians can move along shared arcs without interference.

Figures 3b and 3d illustrate the evacuation flows of pedestrians and vehicles from non-retrofitted sub-zones $o2$, $o4$, and $o5$. As shown in Figure 3b, pedestrians in sub-zone $o5$ are assigned to horizontal shelter $h1$, which is the only shelter within the acceptable tolerance limit. Considering the slope, they can reach $h1$ in two minutes. The lead time for this arc is determined as the minimum of the lead times of its tail and head nodes (8 and 9 minutes), resulting in an effective lead time of 8 minutes. Since the travel time is two minutes and the arc has no capacity constraint, evacuees can safely reach the shelter even if they depart at minute five. Pedestrians in sub-zone $o4$ are assigned to vertical shelter $v3$, which is within the tolerance limit and has sufficient capacity (q_{v3}) under the available budget. Although shelter $v4$ is also within reach (two minutes away), it poses higher risk as it leads toward the shoreline; hence, $v3$ is prioritized. For pedestrians in sub-zone $o2$, if no vertical shelters are available, they cannot reach any horizontal shelter before the inundation time (since the sum of travel and departure times equals nine minutes). Therefore, they are assigned to one of the candidate vertical shelters $v1$ or $v2$, both within the tolerance limit. Between the two, opening $v1$ is preferred given its proximity and lower risk, but its limited capacity may result in some unmet demand—indicating a bottleneck. If no budget is available to open additional shelters, the unsheltered evacuees from $o2$ are directed to dummy nodes, representing unmet demand. Overall, all pedestrians in non-retrofitted sub-zones are assumed to be fully compliant, as they are assigned to shelters within the tolerance radius.

In the vehicular evacuation illustrated in Figure 3d, the only destination type is the horizontal shelter. Although horizontal shelters have unlimited capacity, the arcs leading to them are capacity-constrained (when referring to an arc a, its capacity is denoted as c_a) and tend to zero as the tsunami waves approach due to inundation. The capacity c_a represents the maximum number of vehicles that can traverse an arc under free-flow conditions. To prevent congestion, the total vehicular flow on each arc must remain below its capacity. Consequently, only a proportion of vehicles from each sub-zone ($\bar{v}_\pi$) are assigned to the shortest-time route to the nearest horizontal shelter π^*_o, while the remaining vehicles (v_π) are assigned to alternative routes to the same or other shelters.

Figure 3d illustrates the compliance behavior of drivers in non-retrofitted sub-zones. In sub-zone $o5$, vehicles are located very close to horizontal shelter $h1$. Since the artificial arcs directly

connecting this sub-zone to surrounding nodes are assumed to have sufficiently large capacity, all vehicles can reach $h1$ within one minute. As the assigned path coincides with the shortest-time route, full compliance is observed ($\alpha^{w}_{r^1_{o5,h1}} = 1$). In sub-zone $o4$, vehicles are assigned to shelter $h1$ through two distinct routes to satisfy all demand given arc capacity constraints. Along the first route, all vehicles comply with the assigned path ($\alpha^{w}_{r^1_{o4,h1}} = 1$), while along the second, only a portion ($\alpha^{w}_{r^2_{o4,h1}}$) follow the assigned path. The remaining drivers ($1 - \alpha^{w}_{r^2_{o4,h1}}$) deviate to the shortest-time path, where they may face delays at certain nodes but can still reach the shelter before inundation. Vehicles from sub-zone $o2$ are assigned to horizontal shelter $h2$ due to congestion on alternative paths. A fraction ($\alpha^{w}_{r^1_{o2,h2}}$) comply with this assignment, while the remainder ($1 - \alpha^{w}_{r^1_{o2,h2}}$) attempt to evacuate via the shortest-time route toward shelter $h1$. However, due to arc congestion, some of these noncompliant vehicles fail to reach $h1$ before inundation and are therefore assigned to dummy nodes, representing unmet demand. These noncompliant drivers contribute to network overcapacity by self-evacuating along the shortest routes despite official instructions.

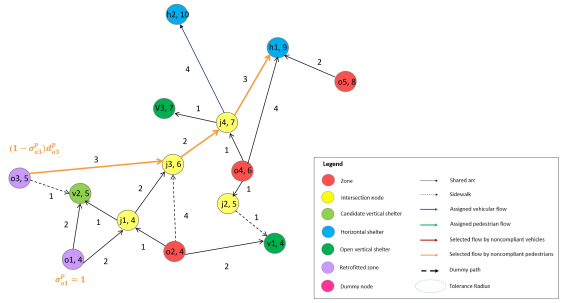

(a) Compliance behavior of pedestrians in retrofitted sub-zones.

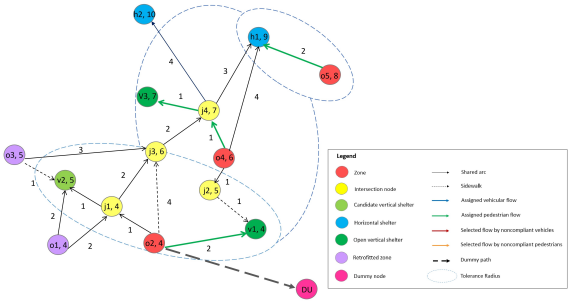

(b) Compliance behavior of pedestrians in non-retrofitted sub-zones.

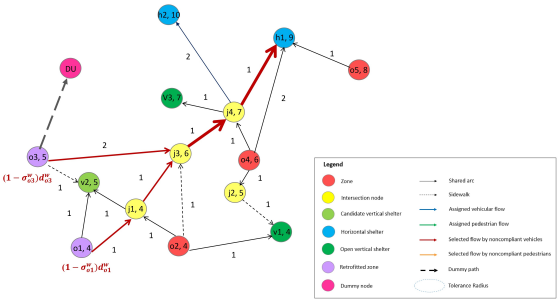

(c) Compliance behavior of vehicles in retrofitted sub-zones.

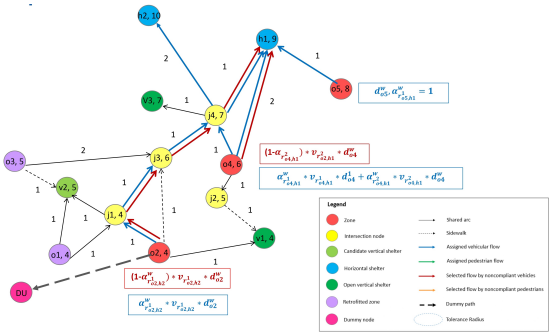

(d) Compliance behavior of vehicles in non-retrofitted sub-zones.

Figure 3: Compliance behaviors of pedestrians and vehicles in retrofitted and non-retrofitted sub-zones.

3.1.1 Time-Expanded Network Construction

The main objective of the evacuation model is to minimize overall risk by ensuring that evacuees reach shelters before tsunami waves inundate nodes and paths, making them unusable. As the tsunami advances, node-specific risk levels increase, and at their respective lead times, nodes and connected arcs become impassable. Each node has its own lead time, rather than assigning a single value to an entire route, which allows the model to reflect spatial variations

in inundation timing. Because these risk levels evolve dynamically, a static network cannot adequately capture temporal changes. To address this, a time-expanded network is constructed to represent the evacuation process over discrete time steps.

In this formulation, the evacuation period is divided into equal time intervals, and a copy of each node is created for every time step during which it remains usable. This structure allows for tracking accessibility over time and directly controlling traffic conditions. Once a node's lead time is reached, it and its associated arcs are removed from the network, representing inundation. Similarly, subzones appear only after their designated departure times—for example, subzones o_1–o_3 depart at time 0, o_4 appears at time 2, and o_5 at time 4.

Two types of arcs are included in the time-expanded network: *crossing arcs* and *holdover arcs*. Crossing arcs connect different nodes across consecutive time steps, representing evacuee movement. Holdover arcs, in contrast, link the same node across consecutive time steps and indicate remaining at that node for a short period. For vehicles, however, holdover arcs are essential, as shown in Figure 4b, since they allow temporary waiting when road capacity is reached, preventing excessive congestion and improving overall evacuation performance. These arcs are not defined for horizontal shelters because vehicles are assumed to complete their evacuation upon arrival at such shelters.

The construction of crossing and holdover arcs is based on three main parameters: travel time, time-step length, and lead time. Travel time depends on the distance and speed between nodes, the time-step length determines the temporal resolution, and the lead time specifies the final time step before a node and its arcs become unusable due to inundation.

Consider the static network discussed earlier, where each node has a defined lead time and each arc has known travel times for both vehicles and pedestrians. Departure times vary among subzones as described above. For instance, the static arc between o_4 and j_3 has a vehicle travel time of one minute, with lead times of six and seven minutes for o_4 and j_3, respectively. Using a one-minute time-step length, the tail of the crossing arc is defined over the interval

$$[\text{departure time}, \text{lead time} - \lceil \text{travel time} \rceil] = [2, 5],$$

and the head over

$$[\lceil \text{departure time} + \text{travel time} \rceil, \text{lead time} - 1] = [3, 6].$$

Thus, multiple crossing arcs can be generated from each static arc depending on the available time intervals. Figure 4a illustrates the generated vehicle crossing arcs.

Holdover arcs are constructed similarly, except their travel time equals the time-step length. For each node, except horizontal shelters, holdover arcs connect two consecutive time steps, enabling vehicles to remain stationary until it becomes feasible to move forward. This captures the accumulation of vehicles at congested nodes and their gradual release once sufficient capacity is available. Figure 4b illustrates these arcs, showing how they manage temporal vehicle flow and alleviate congestion.

For pedestrians, the same principle is applied to create crossing arcs, with the difference that vertical shelters are also included since pedestrians can access them directly. As pedestrian arcs are not subject to capacity constraints, waiting is unnecessary, and holdover arcs are therefore not defined for pedestrians.

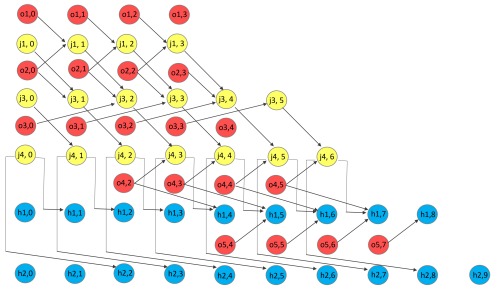

(a) Generated crossing arcs.

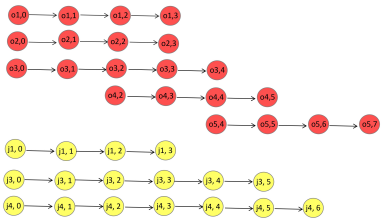

(b) Generated holdover arcs.

Figure 4: Generated crossing and holdover arcs in the time-expanded network for vehicles.

3.1.2 Assumptions

1. The tsunami is assumed to occur during nighttime, when background traffic is negligible and set to zero.

2. Evacuees traveling by private vehicles aim solely to leave the inundation area and do not seek refuge in vertical shelters, while pedestrians may be assigned to either vertical or horizontal shelters.

3. The available budget is allocated to retrofitting existing buildings and to constructing or retrofitting vertical shelters.

4. When the shelter-in-place (SIP) strategy is adopted for a sub-zone, all residential buildings within that zone are assumed to have been retrofitted, and each retrofitted building has sufficient capacity to accommodate its inhabitants, ensuring that the infrastructure can safely sustain all occupants during a disaster.

5. Vertical shelters are assumed to have finite capacities, whereas horizontal shelters have unlimited capacity. The capacity of vehicle crossing arcs is limited, while pedestrian arcs are considered unconstrained.

6. The risk associated with staying in horizontal shelters is assumed to be zero, implying that they offer complete safety. However, the risk of staying in vertical shelters is incorporated into the travel risk calculation.

7. The departure times may differ across sub-zones, but pedestrians and vehicles within each subzone depart at the same time.

8. All personal vehicles are assumed to have identical capacity and velocity.

9. Pedestrians have an initial walking speed of 1 m/s, which varies with the slope of the road. Based on González-Riancho et al. (2013), a speed correction factor is applied to adjust pedestrian velocity according to road gradient.

10. Since tsunamis occur following earthquakes, the capacities of arcs are assumed to decrease according to the building damage levels provided in the *Estimated Earthquake Losses by Districts in Istanbul* report (İBB, 2023).

11. All evacuees, whether pedestrians or vehicle users, are evacuated through arcs filtered by direction. Only arcs leading away from the coastline are considered valid. For instance, in the example network shown in Figure 5, the red line represents the coastline, and two directed arcs, A–B and C–D, are illustrated. Arc A–B is accepted since node B is farther from the coastline than node A, guiding evacuees inland. In contrast, arc C–D is rejected because node D is closer to the coastline than node C, directing evacuees toward the shore.

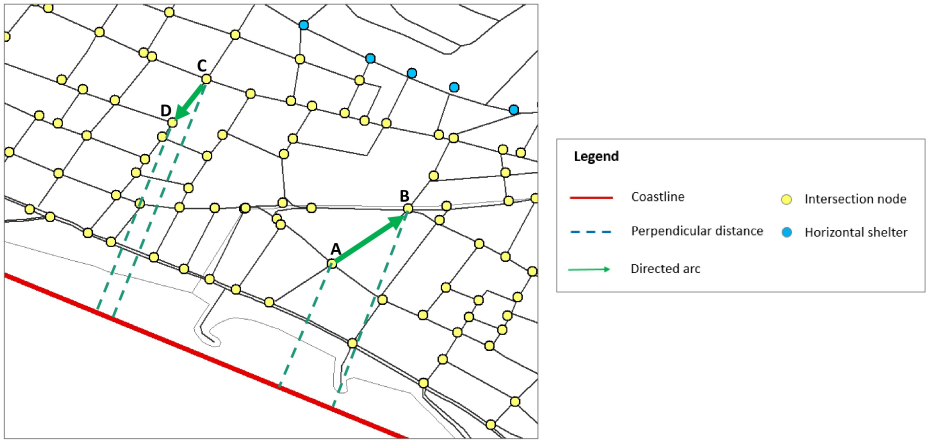

Figure 5: Example of arc filtering based on direction relative to the coastline.

3.2 Model Reformulation

Table 1: Notations of model

Sets	
O	Set of evacuation zones
J	Set of junction nodes
S	Set of shelters where $S^v \cup S^h = S$
S^v	Subset of candidate locations for vertical shelters construction
S^h	Subset of horizontal shelters
S_o^ϵ	Set of candidate vertical shelters within tolerance degree where $S_o^\epsilon \subseteq S^v$
A	Set of possible arcs A where $A^v \cup A^p = A$
A^w	Subset of arcs that can be used by vehicles and pedestrians
A^p	Subset of arcs that can be used only by pedestrians (sidewalks)
Π	Set of routes between zones and shelters
$\Pi_{o,s}$	Set of routes between origin zone o and shelter s within tolerance degree
Π_o^*	Set of shortest-time routes for vehicles at zone o
π_o^*	Shortest route for pedestrians at zone o
Π_a	Set of routes of which a is a part where $P_a \subseteq P$
A_π	Set of arcs on route π where $A_\pi \subseteq A$
Parameters	
h_s	Cost of constructing shelter s, $\forall s \in S^v$
f_o	Fixed cost of retrofitting residential building of evacuation zone o, $\forall o \in O$
r_π	Total risk that vehicles incur on route π, $\forall \pi \in \Pi_{o,s}$
$r_{o,s}$	Total risk that pedestrian incur during traveling from zone o to shelter s,$\forall o \in O, s \in S^v$ risk of staying in vertical shelters are included
r_o	Risk of staying at home (sheltering in place)for evacuees of zone o, $\forall o \in O$
r_s	Risk (penalty) for extended capacity of shelter s, $\forall s \in S^v$
α_o^{w,t_π}	Compliance rate of vehicles from zone o in taking route π, based on the arrival-time difference t between the suggested route and the shortest-time route, $\forall o \in O$.
σ_o^w	Compliance rate of vehicles from zone o with shelter in place, $\forall o \in O$
σ_o^p	Compliance rate of pedestrians from zone o with shelter in place, $\forall o \in O$
d_o^w	Evacuation demand for vehicles in zone o, $\forall o \in O$
d_o^p	Evacuation demand for pedestrians in zone o, $\forall o \in O$
q_s	Capacity of shelter s, $\forall s \in S^v$
c_a	Capacity of arc a, $\forall a \in A^v$
B	Budget for retrofitting the building and opening vertical shelters
variables	
e_o	1 if zone o is evacuated, 0 if zone o is retrofitted against tsunami, $\forall o \in O$
y_s	1 if potential location s is selected for construction of the shelter in, 0 otherwise, $\forall s \in S^v$
$z_{o,s}$	1 if shelter s is assigned to pedestrians of zone o, 0 otherwise, $\forall o \in O, s \in S^v$
v_π	Fraction of vehicles evacuated through route π (between evacuation node o and shelter s) $\forall \pi \in \Pi_{o,s}$
$\bar{v}_\pi$	Fraction of vehicles in evacuation zone o select the shortest-time route $\forall \pi \in \Pi_o^*$
u_s	Number of pedestrians who do not fit in shelters s (extended capacity) ,$\forall s \in S^v$

$$Min\Bigg(\sum_{o\in O}\sum_{s\in S^h}\sum_{\pi\in\Pi_{o,s}} r_\pi \alpha_o^{w,t_\pi} d_o^w v_\pi + \sum_{o\in O}\sum_{\pi\in\Pi_o^*} r_\pi d_o^w \bar{v}_\pi + \sum_{o\in O} r_{\pi_o^*} d_o^p (1-\sigma_o^p)(1-e_o) + \sum_{o\in O}\sum_{s\in S_o^\epsilon} r_{o,s} d_o^p z_{o,s} + \sum_{o\in O} r_o d_o^w \sigma_o^w (1-e_o) + \sum_{o\in O} r_o d_o^p \sigma_o^p (1-e_o) + \sum_{s\in S^v} r_s u_s\Bigg) \tag{11}$$

$$\sum_{o\in O} f_o(1-e_o) + \sum_{s\in S^v} h_s y_s \le B \tag{12}$$

$$\sum_{s\in S^h}\sum_{\pi\in\Pi_{o,s}} \alpha_o^{w,t_\pi} v_\pi + \sum_{\pi\in\Pi_o^*} \bar{v}_\pi = 1-\sigma_o^w(1-e_o) \quad \forall o\in O \tag{13}$$

$$\sum_{s\in S^h}\sum_{\pi\in\Pi_{o,s}} v_\pi \le e_o \quad \forall o\in O \tag{14}$$

$$\sum_{o\in O}\sum_{s\in S^h}\sum_{\pi\in\Pi_a\cap\Pi_{o,s}} \alpha_o^{w,t_\pi} d_o^w v_\pi + \sum_{o\in O}\sum_{\pi\in\Pi_o^*\cap\Pi_a} d_o^w \bar{v}_\pi \le c_a \quad \forall a\in A^v \tag{15}$$

$$\sum_{s\in S_o^\epsilon} z_{o,s} = e_o \quad \forall o\in O \tag{16}$$

$$\sum_{\substack{s\in S:\\ l_{o,s}>(1+\epsilon)l_{o,s'}}} z_{o,s} + y_{s'} \le 1 \quad \forall o,s'\in S^v \tag{17}$$

$$\sum_{o\in O} d_o^p z_{o,s} \le q_s y_s + u_s \quad \forall s\in S^v \tag{18}$$

$$u_s \le \sum_{o\in O} d_o^p y_s \quad \forall s\in S^v \tag{19}$$

$$v_\pi, \bar{v}_r, u_s \ge 0, e_o, y_s, z_{o,s} \in \{0,1\} \tag{20}$$

The objective of the model is to minimize the total risk associated with the evacuation process. The first term represents the risk of compliant vehicles traveling along their assigned routes, while the second accounts for non-compliant vehicles that disregard shelter-in-place orders in retrofitted zones or ignore assigned routes in non-retrofitted zones, instead selecting their own shortest path. In the time-expanded network, no single shortest path exists, as capacity limits at intermediate nodes may create multiple alternatives; this term captures that risk. The third term reflects the risk of non-compliant pedestrians who ignore shelter-in-place and evacuate to the nearest horizontal shelter, where paths are unique due to the absence of pedestrian arc capacity constraints. The fourth and fifth terms capture the residual risk for compliant evacuees—both

pedestrians and vehicles—who remain at home after retrofitting, while the final term penalizes expanded shelter capacity, treated as unsatisfied demand.

Constraint 12 imposes the budget limitation for retrofitting buildings and opening vertical shelters. According to Constraints 13 and 14, vehicle assignment depends on the retrofitting status of each zone: in retrofitted zones ($e_o = 0$), there will be no assignment; in non-retrofitted zones ($e_o = 1$), vehicles are assigned to horizontal shelters, with a fraction of evacuees—depending on the compliance rate—following the suggested routes and the remainder selecting the shortest-time path. Constraint 15 enforces arc capacities considering both compliant and non-compliant vehicle flows. Constraint 16 prevents assigning pedestrians from retrofitted zones to any shelter, whereas pedestrians from non-retrofitted zones must be evacuated to exactly one shelter, vertical or horizontal. Constraint 17 incorporates pedestrian distance tolerance by requiring that, if a vertical shelter is open, assignments do not exceed $(1+\epsilon)$ times the shortest path length, ensuring full compliance. Constraint 18 restricts inflows to vertical shelters to their allowed capacity, including possible capacity expansion, while Constraint 19 ensures that capacity expansion is permitted only if the shelter itself is open. Finally, Constraint 20 specifies the domains of all decision variables.

4 Solution Methodology

The Nested Benders–Column Generation Decomposition method was developed to solve the proposed model. The framework is based on Benders decomposition, which partitions the problem into a master problem and a subproblem. To efficiently address the exponential number of candidate routes, column generation is embedded within the subproblem. In addition, acceleration strategies are incorporated to strengthen cuts and expedite convergence.

4.1 Benders Decomposition Framework

The decomposable structure of the MILP model makes it well-suited for Benders Decomposition (BD). By exploiting this structure, BD enables an efficient solution approach by partitioning the problem into a master problem and a subproblem. The master problem captures strategic decisions such as retrofitting buildings, opening vertical shelters, and assigning pedestrian routes, while the subproblem focuses on optimizing vehicular routes and expanding shelter capacities to accommodate evacuees. The master problem is formulated as follows:

Master Problem (MP)

$$\begin{aligned} Min \quad & \Big(\phi^w + \phi^p + \sum_{o\in O} r_o d_o^w \sigma_o^w (1-e_o) + \sum_{o\in O} r_{\pi_o^*} d_o^p (1-\sigma_o^p)(1-e_o) + \\ & \sum_{o\in O}\sum_{s\in S_o^\epsilon} r_{o,s} d_o^p z_{o,s} + \sum_{o\in O} r_o d_o^p \sigma_o^p (1-e_o)\Big) \end{aligned} \tag{21}$$

$$\sum_{o\in O} f_o(1-e_o) + \sum_{s\in S^v} h_s y_s \le B \tag{22}$$

$$\sum_{s\in S_o^\epsilon} z_{o,s} = e_o \quad \forall o \in O \tag{23}$$

$$\sum_{\substack{s\in S:\\ l_{o,s}>(1+\epsilon)l_{o,s'}}} z_{o,s} + y_{s'} \leq 1 \quad \forall o, s' \in S^v \tag{24}$$

$$\phi^w \geq \sum_{o\in O} \big(1 - \sigma_o^w(1-e_o)\big)\tau_o + \sum_{o\in O} e_o\mu_o + \sum_{a\in A_\pi^v} c_a\gamma_a \tag{25}$$

$$\phi^p \geq \sum_{s\in S^v} \left(\big(q_s y_s - \sum_{o\in O} d_o^p z_{o,s}\big)\rho_s + \sum_{o\in O} d_o^p \bar{y}_s \theta_s \right) \tag{26}$$

$$e_o, y_s, z_{o,s} \in \{0,1\}, \phi^1, \phi^2 \geq 0 \tag{27}$$

To account for the distinct characteristics of pedestrians and vehicles, the subproblem is further decomposed into two components: a pedestrian subproblem (SPP) and a vehicle subproblem (SPV). This separation ensures that their respective constraints are handled independently, while also enhancing computational efficiency by producing more compact formulations that are easier to solve and can be addressed in parallel. The primal subproblems are formulated as follows:

Primal Sub-problem for pedestrians $(PSPP)$

$$Min \sum_{s\in S^v} r_s u_s \tag{28}$$

$$\sum_{o\in O} d_o^p \bar{z}_{o,s} \leq q_s \bar{y}_s + u_s \quad \forall s \in S^v \tag{29}$$

$$u_s \leq \sum_{o\in O} d_o^p \bar{y}_s \quad \forall s \in S^v \tag{30}$$

$$u_s \geq 0 \tag{31}$$

Primal Sub-problem for vehicles$(PSPV)$

$$Min \sum_{o\in O}\sum_{s\in S^h}\sum_{\pi\in\Pi_{o,s}} r_\pi \alpha_o^{w,t_\pi} d_o^w v_\pi + \sum_{o\in O}\sum_{\pi\in\pi_o^*} r_\pi d_o^w \bar{v}_\pi \tag{32}$$

$$\sum_{s\in S^h}\sum_{\pi\in\Pi_{o,s}} \alpha_o^{w,t_\pi} v_\pi + \sum_{\pi\in\Pi_o^*} \bar{v}_\pi = 1 - \sigma_o^w(1-\bar{e}_o) \quad \forall o \in O \tag{33}$$

$$\sum_{s\in S^h}\sum_{\pi\in\Pi_{o,s}} v_\pi \leq \bar{e}_o \quad \forall o \in O \tag{34}$$

$$\sum_{o\in O}\sum_{s\in S^h}\sum_{\pi\in\Pi_a\cap\Pi_{o,s}} \alpha_o^{w,t_\pi} d_o^w v_\pi + \sum_{o\in O}\sum_{\pi\in\Pi_o^*\cap\Pi_a} d_o^w \bar{v}_\pi \le c_a \quad \forall a \in A^v \tag{35}$$

$$v_\pi, \bar{v}_\pi \ge 0 \tag{36}$$

Feasibility issues may arise in the pedestrian subproblem because, in the master problem, pedestrians can be assigned to vertical shelters that are not opened. Since the opening decision is enforced only in the subproblem, such assignments can result in infeasibility. This issue is resolved by introducing the following constraint directly into the master problem instead of generating a feasibility cut:

$$\sum_{o\in O} z_{o,s} \le g\, y_s \quad \forall s \in S^v \tag{37}$$

Where $g = |O|$ denotes the total number of origin zones.

4.2 Column Generation Framework

In the proposed model, it is assumed that a set of candidate routes for compliant drivers and a set of shortest-time paths for noncompliant drivers are available. Enumerating all such routes is typically impractical due to excessive memory requirements and computational intractability, highlighting the need for an efficient solution strategy. To overcome this challenge, Column Generation (CG) is employed, where the vehicular subproblem is decomposed into three components: the Restricted Master Problem (RMP) and two Pricing Problems (PPI and PPII), which generate routes for compliant and noncompliant drivers, respectively. The RMP is solved over a restricted subset of routes, and the Pricing Problems are iteratively solved to identify new routes with negative reduced cost. These routes are then added to the RMP, and the process is repeated until no further routes with negative reduced cost are identified.
The RMP is structurally identical to the vehicular subproblem (SPV), but it is initialized with only a subset of routes. To expand this set, two Pricing Problems (PPI and PPII) are introduced within the column generation framework. In the first column generation, the columns correspond to the variables v_k, while in the second they correspond to $\bar{v}_\pi$. Both PPI and PPII are formulated as Elementary Shortest Path Problems (ESPP), consistent with recent approaches by Yıldırım and Yıldız (2021); Bayram et al. (2022). In the first case, routes are generated between sub-zones and feasible horizontal shelters, while in the second, although the static shortest path for noncompliant drivers in each sub-zone is predetermined, capacity constraints may cause waiting at intermediate nodes, leading to alternative realizations of the path. In both cases, the optimal route is defined as the one with the minimum total cost, computed as the sum of the costs of the included arcs, and identified using the Bellman–Ford algorithm. Any route with negative reduced cost is considered potentially profitable. The formulations of PPI and PPII are given as follows:
(PPI)

$$Min \quad rc^1_{o,s} = \sum_{a\in A^v_{o,s}} \Big(d_o^w r_a x_a - \alpha_o^{w,t_\pi}\big((\tau_o + d_o^w\gamma_a)x_a\big)\Big) - \sum_{a\in A^v_o} \mu_o x_a \tag{38}$$

$$\sum_{a\in\delta^+(i)} x_a(\omega) - \sum_{a\in\delta^-(i)} x_a(\omega) = \begin{cases} 1 & \text{if} \quad i = o \\ 0 & if \quad i \in N\backslash\text{(o,s)} \\ -1 & if \quad i = s \end{cases} \tag{39}$$

$$x_a(\omega) \in \{o, 1\} \tag{40}$$

(PPII)

$$Min \quad rc^2_{o,s} = \sum_{a\in A^*_{o,s}} d^w_o\big(r_a x_a - \gamma_a\big) - \sum_{a\in A^*_o} \tau_o x_a \tag{41}$$

$$\sum_{a\in\delta^+(i)} x_a(\omega) - \sum_{a\in\delta^-(i)} x_a(\omega) = \begin{cases} 1 & \text{if} \quad i = o \\ 0 & if \quad i \in N\backslash\text{(o,s)} \\ -1 & if \quad i = s \end{cases} \tag{42}$$

$$x_a(\omega) \in \{o, 1\} \tag{43}$$

Here, X_a is a binary variable indicating whether arc a is included in route k, and the objective function minimizes the total cost as the sum of the selected arcs. In PPI, the costs are directly linked to the dual multipliers of the compliant vehicle-related constraints (33–35), while in PPII, the costs are associated with the dual multipliers of constraints (33 and 35) obtained from solving the RMP. Specifically, τ_o, γ_a, and μ_o denote the dual multipliers corresponding to Constraints 33–35, respectively. The overall methodological framework of the study is illustrated in Figure 6.

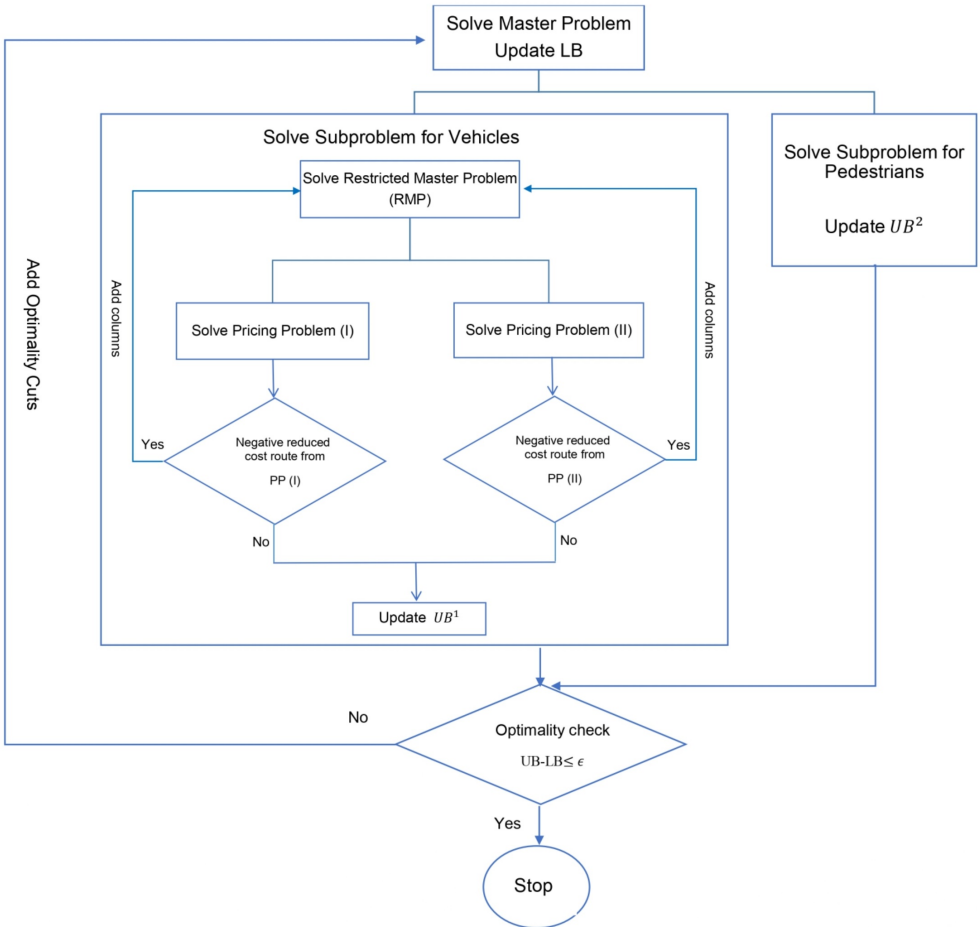

Figure 6: Methodological framework of the proposed solution approach.

In summary, the proposed solution combines Benders Decomposition with Column Generation and proceeds in sequential steps. First, the master problem (MP) is solved to update the lower bound (LB). Next, the pedestrian subproblem (SPP) is solved to obtain dual variables and update the upper bound (UB_2). For the vehicle subproblem (SPV), Column Generation is employed: the restricted master problem (RMP) is solved to generate dual variables, which update arc weights in pricing problems I and II (PPI and PPII). Both pricing problems are solved using the Bellman–Ford algorithm, and any paths with negative reduced cost are added as new routes. This iterative process continues until no further beneficial routes are generated. The final dual variables are then used to compute UB_1, and the overall upper bound is determined as $UB = UB_1 + UB_2$. Finally, optimality is checked: if $UB - LB \geq \epsilon$, optimality cuts for both pedestrians and vehicles are added; otherwise, the algorithm terminates.

4.3 Acceleration methods

The classical Benders decomposition method often suffers from slow convergence due to two main factors. First, weak, redundant, or insufficiently tight cuts can lead to a large number of iterations before convergence. Second, each iteration is computationally intensive, as it requires solving both the master and subproblems. Together, these factors limit efficiency and highlight the need for acceleration techniques to improve convergence performance.

4.3.1 Subproblem Decomposition

In the Benders decomposition framework, the master problem defines strategic decisions such as retrofitting zones, constructing vertical shelters, and assigning pedestrians to shelters, while the subproblem focuses on route assignment for vehicles and unmet pedestrian demand arising from capacity limitations. As pedestrian and vehicle decisions are independent and no shared constraint exists in the subproblem, it is divided into two parts: one for pedestrians (SPP) and one for vehicles (SPV). This separation enables parallel computation and accelerates convergence, enhancing the overall efficiency of the algorithm.

4.3.2 Network Size Reduction for Vehicles

To accelerate the solution process, the vehicular network was streamlined through several reductions. First, origin–destination (O–D) pairs with zero compliance rates or those unreachable in the static network were excluded. Second, node lead times were adjusted, and nodes appearing after their lead time were removed. Directional filtering was also applied, while vertical shelters and pedestrian-related arcs were eliminated.

For compliant drivers, a feasible arc set was constructed for each O–D pair by considering lead times, departure times, and path existence. Arcs involving nodes that appear after the destination's lead time or connected to other horizontal shelters were removed. Arcs were retained only if the time of their head and tail nodes did not exceed the corresponding departure time. Additionally, for each arc, the existence of valid paths was verified from the origin to its start or end node and from these nodes to the destination; arcs failing these conditions were removed.

For noncompliant drivers, feasible arcs for each subzone were determined based on static arcs along the shortest-time path. Corresponding time-dependent arcs, including crossing and holdover arcs, were then generated while accounting for the destination's lead time and the sub-zone's departure time.

4.3.3 Maximum Density Cut (MDC)

The classical Benders decomposition can produce sparse optimality cuts that involve only a few master variables, which slows convergence. The Covering Cut Bundle (CCB) approach counters this by generating a set of cuts so that each variable is α-covered—its coefficient magnitude *in the cut* is at least an α-fraction of the maximum coefficient magnitude *in the cut*, with $\alpha \in (0, 1)$. Constructing a full bundle, however, can be computationally demanding.

To overcome this limitation, we employ a Maximum Density Cut (MDC) strategy that concentrates the densification step on the coefficients of the $z_{o,s}$ variables while preserving dual optimality. Let ρ_s and θ_s denote the dual variables associated with constraints (29) and (30) of the primal subproblem, respectively (both nonpositive in our formulation). MDC exploits degeneracy: among multiple dual-optimal solutions, the auxiliary dual subproblem$_{\underline{z}}$ selects an *extreme point* with the largest support (i.e., the maximum number of nonzero dual variables—particularly in ρ), which yields richer coefficient patterns and faster convergence.

Operationally, the subproblem$_{\underline{z}}$ enforces the full dual-objective equality to remain on the dual-optimal face and introduces only the z-side activation indicators $k^1_{o,s}, k^2_{o,s} \in [0, 1]$ for uncovered pairs (o, s). With a sufficiently large M and a user-chosen threshold $c' > 0$, the big-M bounds ensure $|-d^p_o \rho_s| \geq c'$ whenever $k^1_{o,s} = k^2_{o,s} = 0$, while the objective $\min \sum_{(o,s)} \left(k^1_{o,s} + k^2_{o,s}\right)$ drives as many coefficients as possible beyond the target. The resulting single high-density optimality cut increases variable coverage and reduces the number

of Benders iterations without sacrificing dual consistency.

$$\min \sum_{o\in O}\sum_{s\in S_o^{\epsilon}} \left(k^1_{o,s} + k^2_{o,s}\right) \tag{44}$$

$$-\rho_s + \theta_s \le r_s \qquad \forall s \in S^v \tag{45}$$

$$\sum_{s\in S^v} \Big[\big(q_s\, \bar{y}_s - \sum_{o\in O} d^p_o\, \bar{z}_{o,s}\big)\rho_s \;+\; \big(\sum_{o\in O} d^p_o\big)\bar{y}_s\, \theta_s \Big] \;=\; ODSPP \tag{46}$$

$$-\,c'\,(1-k^1_{o,s}) - M\,k^1_{o,s} \;\le\; -\,d^p_o\,\rho_s \;\le\; -\,c'\,(1-k^1_{o,s}) + M\,k^1_{o,s} \qquad \forall (o,s) \in NCZ \tag{47}$$

$$c'\,(1-k^2_{o,s}) - M\,k^2_{o,s} \;\le\; -\,d^p_o\,\rho_s \;\le\; c'\,(1-k^2_{o,s}) + M\,k^2_{o,s} \qquad \forall (o,s) \in NCZ \tag{48}$$

$$k^1_{o,s} + k^2_{o,s} \le 1 \qquad \forall o \in O,\; s \in S^v \tag{49}$$

$$0 \le k^1_{o,s},\, k^2_{o,s} \le 1, \qquad \rho_s \le 0,\; \theta_s \le 0 \qquad \forall o \in O,\; s \in S^v \tag{50}$$

For further methodological details and variants, see (Saharidis and Ierapetritou, 2013; Jenabi et al., 2015).

4.3.4 Warm Start Strategies

To improve computational efficiency, several acceleration methods are introduced for the Benders decomposition algorithm. Among them, four warm-start strategies are proposed to generate initial feasible solutions that stabilize early iterations and reduce convergence time. Each strategy defines an initial version of the master problem to be solved in the first iteration before proceeding with the standard Benders procedure.

Warm Start Strategy I Since the master problem loses key linking constraints such as shelter capacities after decomposition, an auxiliary master problem is solved only in the first iteration to provide a stronger starting point. In this formulation, shelter capacities and an auxiliary expanded-capacity variable are incorporated to enhance convergence, while all other constraints remain unchanged. The objective function includes the original risk of pedestrians and vehicles, along with the risk of the auxiliary expanded capacity—treated as unsatisfied demand—to maintain consistency with the overall risk structure. As no optimality cuts exist yet, ϕ^p and ϕ^v are set to zero. The resulting solution serves as the initial point for subsequent iterations of the main Benders procedure. The auxiliary master problem is given as follows:

$$\begin{aligned} Min \quad & \Big(\sum_{o\in O} r_o d^w_o \sigma^w_o (1-e_o) + \sum_{o\in O} r_{\pi^*_o} d^p_o (1-\sigma^p_o)(1-e_o) + \\ & \sum_{o\in O}\sum_{s\in S_o^{\epsilon}} r_{o,s} d^p_o z_{o,s} + \sum_{o\in O} r_o d^p_o \sigma^p_o (1-e_o) + \sum_{s\in S^v} r_s u'_s \Big) \end{aligned} \tag{51}$$

$$\sum_{o\in O} d^p_o z_{o,s} \le q_s y_s + u'_s \quad \forall s \in S^v \tag{52}$$

Warm Start Strategy II Since the master problem loses vehicle-related risk information after decomposition, this strategy is introduced to provide a more informative initialization. In the second warm-start strategy, arc-capacity and routing-compliance constraints for vehicles are relaxed, while the formulation for pedestrians remains identical to that in the first strategy. Each origin o is assigned to a single shortest-time path under fully arc-capacity–relaxed conditions, denoted by λ_o. For origins that cannot reach any horizontal shelter even under these conditions and have not been retrofitted due to budget limitations, λ_o represents a dummy path with high risk corresponding to unsatisfied demand. Consequently, all vehicles are treated as fully compliant with routing, whereas shelter-in-place non-compliance is still considered: if an origin has no access, all evacuees are fully compliant; if it has access, *all evacuees in the subzones* use the shortest-time path for the zone λ_o, in which case no dummy path is involved. The objective function therefore incorporates the risk of assigning vehicles to either the shortest-time path or the dummy path, together with the shelter-in-place non-compliance risk, while all other components and constraints remain identical to those in Strategy I. The formulation of this auxiliary master problem (AMP II) is given as follows:

$$\begin{aligned} Min \quad & \Big(\sum_{o\in O} r_o d_o^w \sigma_o^w (1-e_o) + \sum_{o\in O} r_{\pi_o^*} d_o^p (1-\sigma_o^p)(1-e_o) + \\ & \sum_{o\in O}\sum_{s\in S_o^\epsilon} r_{o,s} d_o^p z_{o,s} + \sum_{o\in O} r_o d_o^p \sigma_o^p (1-e_o) + \sum_{s\in S^v} r_s u_s' + \sum_{o\in O} r_{\lambda_o} d_o^w (1-\sigma_o^w)(1-e_o) + \sum_{o\in O} r_{\lambda_o} d_o^w e_o \Big) \end{aligned} \tag{53}$$

Warm Start Strategy III This strategy is similar to Warm Start Strategy II: arc-capacity limits remain relaxed and routing compliance is enforced, while the pedestrian formulation is unchanged. Non-compliant drivers in retrofitted zones follow the shortest-time route λ_o. For each origin o, let β_o denote the candidate set of capacity-relaxed shortest-time routes to distinct reachable shelters in the static network (no waiting); if no shelter is reachable, set $\beta_o = \{\text{dummy}\}$. Introduce an auxiliary binary variable x_{b_o} for $b_o \in \beta_o$, where $x_{b_o} = 1$ if route r_o is selected, and enforce a single choice via $\sum_{b_o\in\beta_o} x_{b_o} = e_o$ (redundant under no arc-capacity limits, but retained for clarity and to serialize the choice in AMP III). For non-retrofitted zones, the selected route may be any $b_o \in \beta_o$ under the rule: if there exists an alternative in β_o with strictly lower risk than the shortest-time route, that alternative is chosen; otherwise the shortest-time route is retained. The updated objective function and additional constraints in AMP III are as follows::

$$\begin{aligned} Min \quad & \Big(\sum_{o\in O} r_o d_o^w \sigma_o^w (1-e_o) + \sum_{o\in O} r_{\pi_o^*} d_o^p (1-\sigma_o^p)(1-e_o) + \\ & \sum_{o\in O}\sum_{s\in S_o^\epsilon} r_{o,s} d_o^p z_{o,s} + \sum_{o\in O} r_o d_o^p \sigma_o^p (1-e_o) + \sum_{s\in S^v} r_s u_s' + \sum_{o\in O} r_{\lambda_o} d_o^w (1-\sigma_o^w)(1-e_o) + \sum_{o\in O}\sum_{b_o\in\beta_o} r_{b_o} d_o^w x_{b_o} \Big) \end{aligned} \tag{54}$$

$$\sum_{b_o\in\beta_o} x_{b_o} = e_o \quad \forall o \in O \tag{55}$$

Column Generation Acceleration Strategies

Two acceleration strategies were implemented to enhance the performance of the column generation procedure. The first strategy, *limited negative reduced cost paths*, is applied to both the first and second column generations. In each iteration, a limited number of paths with negative

reduced costs are identified for each zone and incorporated into the Restricted Master Problem (RMP). This selective inclusion broadens the column set while maintaining computational efficiency.

The second strategy, *initial solution (warm start)*, is specific to the initialization of each column generation. For the first column generation, three sets of initial paths are identified for each subzone in the time-expanded network: (1) the $K = 10$ least-risk paths, (2) the $K = 10$ shortest-time paths—both obtained using Dijkstra's algorithm—and (3) the routes generated through a greedy search. In the greedy search, zones and their candidate paths are sorted in ascending order based on their distance from the seashore and associated risk level, respectively. For each zone, the *minimum capacity of arcs* along the shortest-time path is checked after subtracting the maximum non-compliance rate, assuming that the entire demand of the zone is assigned to that path. When the minimum capacity cannot accommodate the total demand, the *arc capacities are updated*, and the next feasible route is evaluated until the demand of the zone is fully satisfied.

For the second column generation, $K = 2$ shortest-time paths are derived based on the static shortest-time route of each subzone, identifying potential paths among nodes along this route that reach destinations at different times within the time-expanded network. Additionally, *dummy paths* are incorporated in both column generations to represent subzones whose evacuees remain at their origin until the lead time, after which they are assigned to a dummy node.

5 Case Study Results

The case study focuses on the *Büyükçekmece District*, located on the European side of Istanbul along the Marmara Sea. This area was selected due to its high tsunami exposure, low-lying topography, and densely populated coastal neighborhoods. For the Marmara region, multiple tsunami scenarios have been defined, with the *Büyükçekmece Submarine Landslide (LSBC) scenario* identified as the most critical for this district. Simulations conducted with the NAMI-DANCE model indicate that LSBC produces relatively high coastal wave heights and short first-wave arrival times. The resulting inundation zone encompasses six neighborhoods classified as high-risk due to their susceptibility to flooding: *Fatih, Atatürk, 19 Mayıs, Dizdariye, Mimar Sinan, and Ulus* (Bayram et al., 2025).

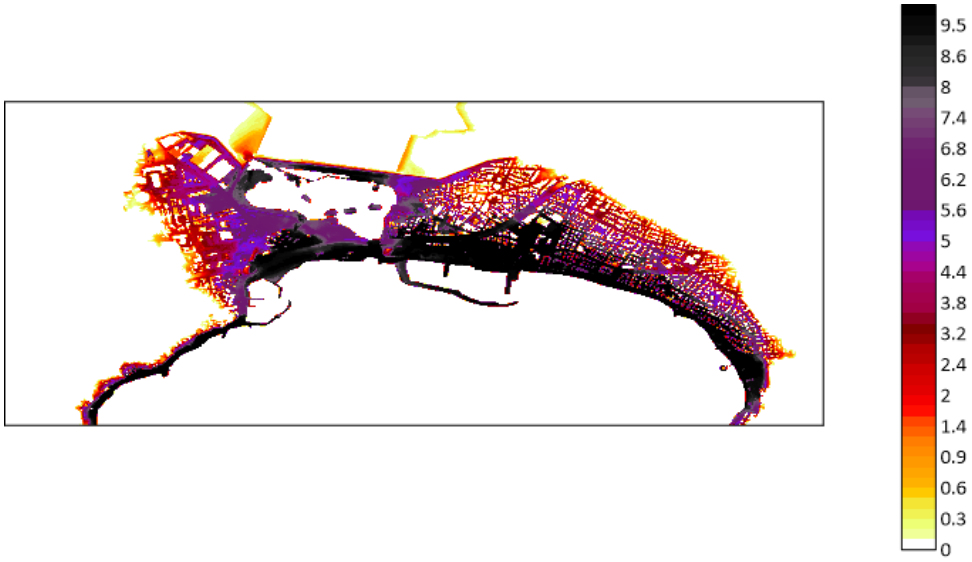

Figure 7: Inundation area under the LSBC scenario in Büyükçekmece (İBB-ODTÜ, 2018, 2019).

The Büyükçekmece network consists of 247 sub-zones, 81 candidate vertical shelters (including 36 existing high-rise buildings), and 67 horizontal shelters. Figure 8 illustrates the spatial layout of the study network.

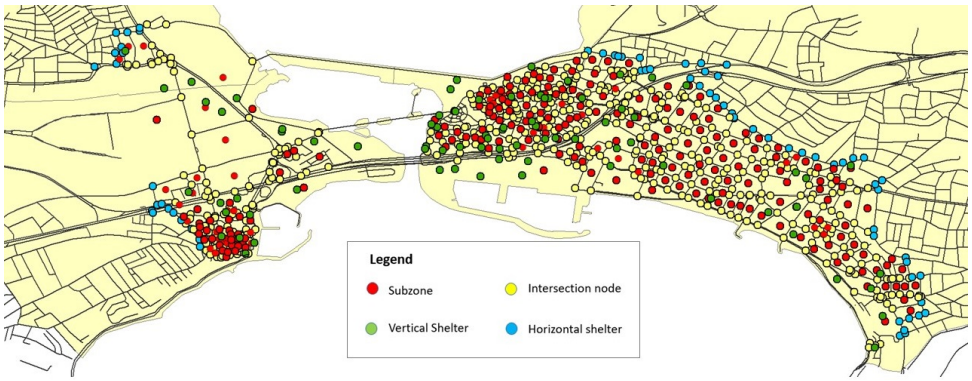

Figure 8: Spatial layout of the Büyükçekmece evacuation network.

5.1 Data Collection

The network components and parameters required for the proposed model were collected as follows:

5.1.1 Evacuation Network

The evacuation network was modeled as a directed graph composed of nodes and road segments. Nodes included sub-zone centroids, intersection points, vertical shelters, and horizontal shelters. Road segments were represented as directed edges and classified as either vehicle roads or sidewalks.

Sub-zones: Sub-zones were defined as rectangular areas enclosed by road segments within the inundation zone.

Vertical Shelters and Capacity: Vertical shelters were identified from existing public buildings, such as hotels and schools, provided that they were structurally stable and had upper floors above the inundation level. Shelter capacity was estimated based on the usable high-floor area located above the inundation depth. In addition, potential new shelters were considered and determined from vacant public lands identified using satellite imagery. For these sites, a standard 6,000 m² design was applied: if the land was smaller, the entire area was used for a single elevated shelter; if larger, only one 6,000 m² shelter was assumed, and the remaining land was unused(Bayram et al., 2025).

Horizontal Shelters: Horizontal shelters were defined as the first intersection nodes located immediately outside the inundation zone, serving as the exit points of evacuation routes.

5.1.2 Evacuation Demand

The evacuation demand for each sub-zone was defined as the product of the number of buildings in the sub-zone, estimated using satellite imagery from Google Maps and Yandex Maps, and the average population per building. The average population per building was calculated by dividing neighborhood population data from the Turkish Statistical Institute (TÜİK, 2021) by the total number of buildings in the neighborhood, as reported by the Istanbul Metropolitan Municipality (İBB, 2017).

5.1.3 Vehicular Demand Ratio

The vehicular demand ratio (VDR) is the proportion of evacuees who evacuate by private vehicle, while the remaining evacuees are assumed to evacuate on foot. Based on a survey of 500 residents in Buyukcekmece (Moslemi et al., 2025), the VDR was estimated at 16%, while 84% of respondents indicated they would walk.

5.1.4 Capacity of Arcs for Vehicles

The capacity of crossing arcs is defined as the maximum number of vehicles that can traverse a road segment within a one-minute time step in the time-expanded network. The base capacity of each vehicle arc is given by (Bayram et al., 2025):

$$\text{Capacity} = \frac{\min\left(L, v \cdot \Delta t\right)}{d_s + l_v} \tag{56}$$

where:

- L: length of the road segment,
- v: free-flow speed,
- $\Delta t = 1$ minute (time step duration),
- $d_s = v \cdot 1\,s$: safety distance,
- l_v: average vehicle length.

To account for infrastructure damage, the base capacity is multiplied by the remaining arc capacity ratio, reflecting the usable road proportion at each damage level. The spatial distribution of damage levels is shown in Figure 9including corresponding remaining ratios.

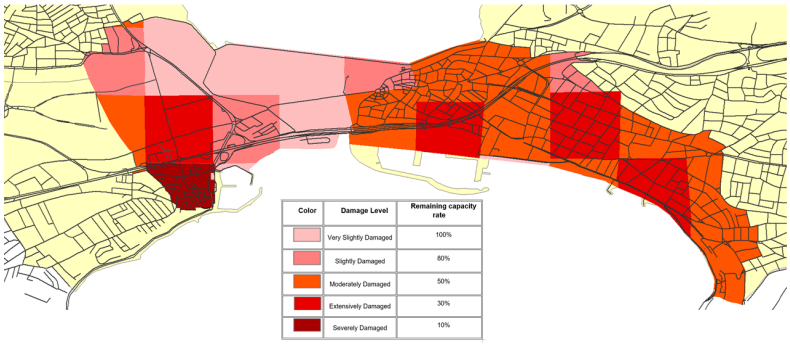

Figure 9: Distribution of road damage levels across the study network(İBB, 2023)

.

For other types of vehicle arcs in the time-expanded network—such as holdover arcs, artificial arcs that connect sub-zone nodes to surrounding nodes, super-exit arcs, and dummy arcs—a very large capacity is assigned to avoid flow restrictions, since these arcs are not physically constrained.

5.1.5 Vehicle Occupancy

Among the survey respondents in Büyükçekmece (Moslemi et al., 2025), the average household size was three persons. Accordingly, the model assumes that each vehicle used during the evacuation carries three occupants.

5.1.6 Pedestrian Tolerance

Pedestrian tolerance captures the maximum distance evacuees are willing to walk to reach a shelter relative to the shortest path. In the survey, respondents were asked to indicate the longest acceptable walking distance within predefined intervals. Figure 10 presents both the raw distribution of responses (left) and the fitted acceptance S-curve (right).

Maximum acceptable distance to nearest shelter or other shelters more than 1 km away

		Frequency	Percent	Valid Percent	Cumulative Percent
Valid	1-3 km	402	80.4	80.4	80.4
	4-6 km	70	14.0	14.0	94.4
	7-8 km	12	2.4	2.4	96.8
	9-10 km	16	3.2	3.2	100.0
	Total	500	100.0	100.0	

(a) Survey responses on maximum acceptable walking distance.

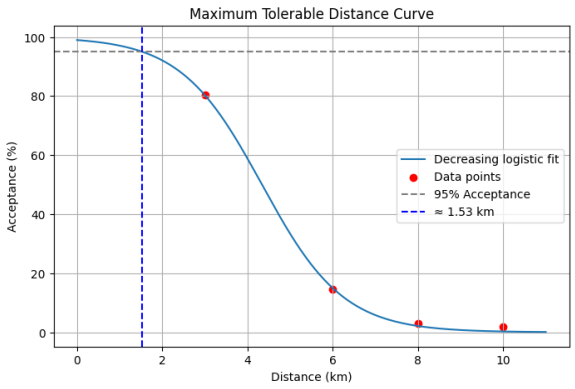

(b) S-curve representing pedestrian tolerance.

Figure 10: Pedestrian tolerance results from the survey (Moslemi et al., 2025).

A decreasing logistic function was then fitted to the cumulative data, representing the probability that evacuees will accept walking a given distance (Moslemi et al., 2025):

$$f(x) = \frac{1}{1 + \exp\left(1.0475 \cdot (x - 4.3401)\right)} \tag{57}$$

From this function, it was estimated that 95% of respondents would accept walking up to 1.53 km. Since the shortest path length is assumed to be 1 km, any route longer than 1.53 times the shortest path is considered unacceptable for pedestrians.

5.1.7 Departure Time

Evacuees require time to complete pre-evacuation activities before leaving home. Survey responses revealed that the majority of residents in Buyukcekmece needed between one and five minutes for preparation before departure (Moslemi et al., 2025). Figure 11(a) presents the distribution of responses, while Figure 11(b) shows the fitted S-curve derived from the cumulative data.

Time to complete actions and depart home (start evacuation)

		Frequency	Percent	Valid Percent	Cumulative Percent
Valid	less than 1 minute	68	13.6	13.6	13.6
	1-5 min	297	59.4	59.4	73.0
	6-10 min	95	19.0	19.0	92.0
	11-20 min	20	4.0	4.0	96.0
	21-30 min	7	1.4	1.4	97.4
	>30 min (more than 30 minutes)	3	.6	.6	98.0
	not applicable	10	2.0	2.0	100.0
	Total	500	100.0	100.0	

(a) Survey responses on pre-evacuation preparation time.

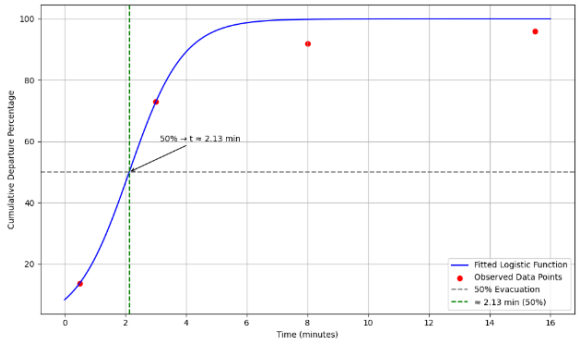

(b) Fitted S-curve for departure time.

Figure 11: Departure time results from the survey(Moslemi et al., 2025).

A logistic function was fitted to this curve to estimate the proportion of residents departing at each time step(Moslemi et al., 2025):

$$f(t) = \frac{1}{1 + \exp(-1.1283 \cdot (t - 2.1255))} \tag{58}$$

Based on this function, it was estimated that all evacuees would have departed by the eighth minute. These estimates were then translated into sub-zone-level departure schedules, with sub-zones ranked according to their distance from the shoreline and those located closer to the coast assigned earlier departure times. Figure 12 illustrates the grouping of sub-zones that depart at each time step between 0 and 8 minutes.

5.1.8 Compliance with Shelter-in-Place

Based on the survey conducted by Moslemi et al. (2025), respondents were asked how likely they would be to remain in their retrofitted buildings during a tsunami event. Answers ranged from *very unlikely* to *very likely*, with the distribution of responses shown in Figure 13(a).

Figure 12: Sub-zones grouped by departure time between 0 and 8 minutes.

To quantify these responses, probabilities were assigned to each category—0.1 for *very unlikely*, 0.3 for *unlikely*, 0.5 for *neutral*, 0.7 for *likely*, and 0.9 for *very likely*—as illustrated in Figure 13(b). The weighted average compliance probability was calculated as 0.7, indicating that approximately 70% of residents would comply and stay in place if their buildings were retrofitted, while 30% would still evacuate.

		Frequency	Percent	Valid Percent	Cumulative Percent
Valid	Very unlikely	1	.2	.2	.2
	Unlikely	55	11.0	11.0	11.2
	Neutral	138	27.6	27.6	38.8
	Likely	38	7.6	7.6	46.4
	Very likely	268	53.6	53.6	100.0
	Total	500	100.0	100.0	

(a) Distribution of survey responses on compliance with shelter-in-place.

Response	Assigned Probability	Frequency
Very unlikely	0.1	1
Unlikely	0.3	55
Neutral	0.5	138
Likely	0.7	38
Very likely	0.9	268

(b) Assigned probabilities for each response category.

Figure 13: Compliance with shelter-in-place based on survey results (Moslemi et al., 2025).

5.1.9 Compliance with Route Assignment

Compliance with route assignment was modeled for vehicles based on survey data reported in distance terms, where participants indicated their maximum acceptable detour to the nearest shelter when the shortest path was one kilometer (Moslemi et al., 2025). These responses were converted into equivalent time differences, rescaled to a 0–15 minute range, and fitted with a logistic function (Equation 59, Figure 14).

		Frequency	Percent	Valid Percent	Cumulative Percent
Valid	1-10	215	43.0	43.0	43.0
	11-20	263	52.6	52.6	95.6
	21-50	14	2.8	2.8	98.4
	51-100	6	1.2	1.2	99.6
	Over 100	2	.4	.4	100.0
	Total	500	100.0	100.0	

(a) Survey responses on maximum acceptable detour (distance).

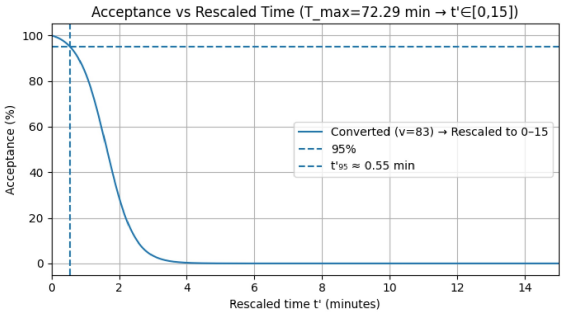

(b) Converted responses into time differences and fitted acceptance curve.

Figure 14: Compliance with vehicle route assignment(Moslemi et al., 2025).

$$f(t) = \frac{1}{1 + \exp\left(0.3663 \cdot (6.6667t - 10.8009)\right)}, \quad 0 \leq t \leq 15 \tag{59}$$

The results show that compliance declines sharply, falling to about 83% when the assigned route is one minute longer than the shortest path and approaching zero by four minutes. Accordingly, only vehicle routes within four minutes of the shortest path were retained, as longer detours would not be realistically accepted.

5.1.10 Risk Assessment

Risk is evaluated using the *MeTHuVA* (METU Metropolitan Tsunami Human Vulnerability Assessment) framework, developed by researchers at METU and applied in the Istanbul Tsunami Action Plan. It is defined as the product of hazard and a composite vulnerability index based on the following factors (Dogan et al., 2021a,b; Tufekci-Enginar et al., 2022):

$$\text{Risk} = H \times \left(\frac{VL}{n \times RE} \right), \tag{60}$$

where

- **Hazard** (H) denotes tsunami intensity, measured from NAMI-DANCE simulations as the maximum flow depth on land for the chosen scenario.
- **Vulnerability at Location** (VL) reflects the fragility of people in a given area, considering land use, geology, landslide-scarp density, elevation, and distance to the shoreline. These sub-factors are aggregated using the Analytic Hierarchy Process.
- **Evacuation Resilience** (RE) represents accessibility to safety, determined by proximity to roads and buildings, road network density, terrain slope, and shoreline distance.
- **Preparedness** (n) captures community awareness and readiness on a scale from 1 to 10, where higher values reduce risk by mitigating vulnerability and resilience constraints.

Beyond this static formulation, time-dependent risk is also computed by integrating dynamic tsunami simulations with vulnerability factors.

5.1.11 Cost Parameters

The following cost parameters were used in the model (Erdurmuş, 2005; Official Gazette, 2023):

- **Construction of new vertical shelters:** 22,500 TL per square meter multiplied by the shelter area.
- **Retrofitting of existing vertical shelters:** 7,500 TL per square meter of usable shelter area.
- **Retrofitting of residential buildings:** 7,500 TL per square meter multiplied by an average building size of 150 m², five floors per building, and five buildings per zone.

5.1.12 Base Budget

It is defined as the minimum funding required to retrofit zones where retrofitting is the only available option to save lives. In our case study, vehicles in 51 zones have no access to horizontal shelters, and pedestrians in 7 zones have no access to either horizontal or vertical shelters. For these 57 zones, retrofitting is the sole feasible intervention; accordingly, the required retrofit cost for these zones constitutes the base budget.

5.2 Computation Results

Several test problems were designed by varying the vehicular demand ratio (VDR) and budget (B) across predefined levels (Table 2). The analysis first focuses on a base-case scenario, in which the vehicular demand ratio is fixed at 16%—as obtained from the survey—and the budget level is set to twice the Base Budget (BB). Subsequently, the results of additional test problems are examined to assess the model's sensitivity to changes in these parameters.

Table 2: Test problem levels for vehicular demand ratio (VDR) and budget (B).

Factor	**Level 1**	**Level 2**	**Level 3**	**Level 4**	**Level 5**
VDR	0%	10%	**16%**	20%	30%
Budget	0	BB	**2×BB**	4×BB	5×BB

5.2.1 Case1: No Evacuation Plan

The first case evaluates the scenario without an organized evacuation plan, providing a baseline against which alternative strategies can be compared. In this case, the available budget is set to zero; consequently, no sub-zone buildings are retrofitted and no vertical shelters are opened. Compliance behavior is also disregarded. Out of the total population of 34,870 in the study area, 18,869 individuals (54.1%) are unable to evacuate, consisting of 14,706 pedestrians and 4,163 vehicle passengers. Among the unsatisfied vehicles, 3,783 passengers are fully unsatisfied in 189 sub-zones, while 304 passengers are partially satisfied in 16 sub-zones. In addition, 76 evacuees are lost due to arc overcapacity. This occurs because compliance behavior is disregarded at the planning stage, but when decisions are adjusted to real-world conditions, noncompliant vehicles appear on the arcs, causing their capacities to be exceeded. These results indicate that vehicles can be fully satisfied in only 37 sub-zones (15%), while unmet pedestrian

demand occurs in 129 sub-zones (53%). The figure 15 shows the spatial distribution of satisfied and unsatisfied pedestrians and vehicles across the network.

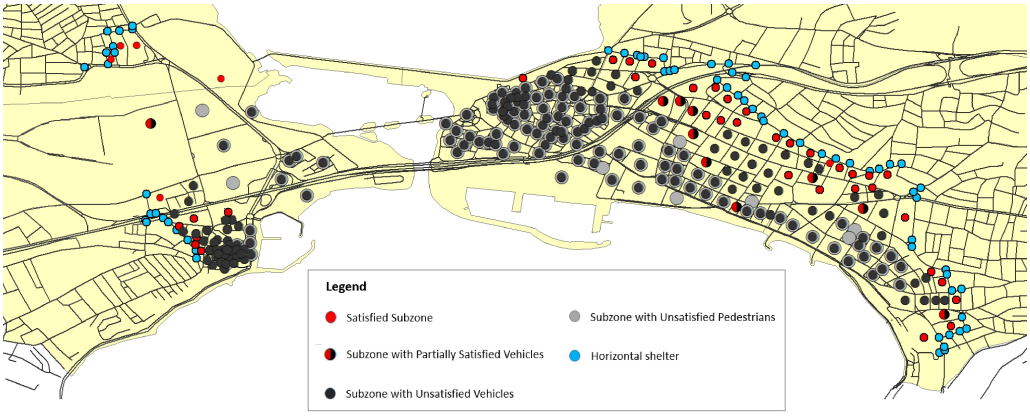

Figure 15: Satisfied and unsatisfied pedestrians and vehicles under the no-plan scenario.

5.2.2 Case 2: Opening Vertical Shelters

In the second case, the entire budget is allocated to opening vertical shelters and, when required, expanding their capacity to identify bottlenecks in the system. In this scenario, 60 out of 81 candidate vertical shelters (74%) are opened, and one shelter requires capacity expansion. Since vertical shelters serve only pedestrians, the number of vehicles unable to evacuate remains unchanged compared to the no-plan case. For pedestrians, however, the improvement is substantial: the number of unsatisfied individuals decreases from 14,706 to 964. Of these, 930 pedestrians in nine sub-zones are unable to evacuate because they cannot reach safety within the available time window, while 34 are unsatisfied due to shelter capacity limitations—individuals who could be saved if vertical shelter capacity were further expanded. Overall, the total population unable to evacuate decreases from 18,869 in the no-plan case to 5,127 (14.7%). These results demonstrate that opening vertical shelters is highly effective in improving pedestrian evacuation outcomes.

Figure 16 illustrates the locations of the opened vertical shelters, including the one requiring capacity expansion. It also shows the distribution of unsatisfied pedestrians and vehicles.

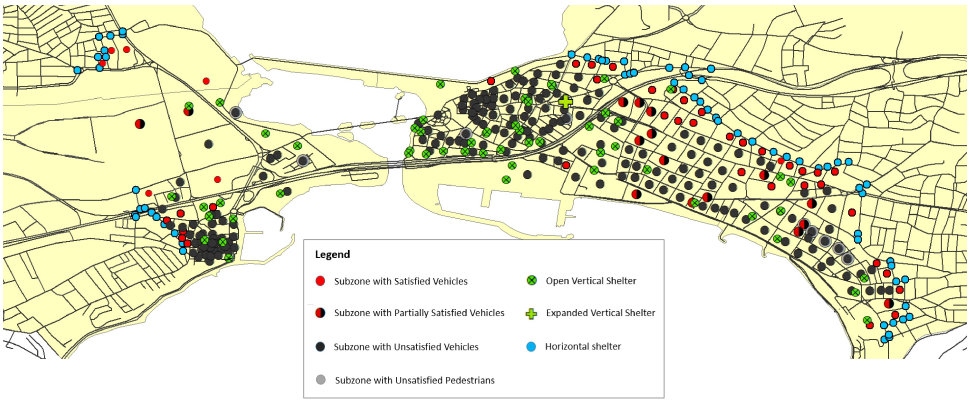

Figure 16: Opened vertical shelters and unsatisfied evacuees in Case 2.

5.2.3 Case 3:Opening Vertical Shelter and Shelter-in-Place

In the third case, the budget is allocated to both opening vertical shelters and retrofitting sub-zones to enable shelter-in-place. A total of 109 sub-zones (44.1%) are retrofitted, while 18 vertical shelters are opened. Retrofitted sub-zones are especially concentrated in areas where shelter-in-place is the only feasible option, though some closer sub-zones are also retrofitted due to factors such as late departure times, limited road capacity, or high population demand. Unlike vertical shelters, retrofitting does not face capacity restrictions and benefits both pedestrians and vehicles. Nevertheless, when pedestrians already have access to vertical shelters within tolerance levels, retrofitting can introduce additional risk. Non-compliant pedestrians, though still able to reach safety, may be exposed to greater tsunami risk than if assigned to vertical shelters, where full compliance is achieved. For vehicles, the situation is more complex: non-compliant drivers leaving retrofitted sub-zones have no alternative but to take their own shortest path, making their risk exposure more difficult to mitigate. By contrast, when sub-zones are not retrofitted, it becomes possible to reduce losses by assigning vehicles to horizontal shelters along routes with higher compliance rates. In some cases, assigning pedestrians to vertical shelters while directing vehicles to horizontal shelters may prove more effective than retrofitting an entire sub-zone. Accordingly, retrofitting and vertical shelters should be regarded as complementary rather than substitutive strategies.

The total number of unsatisfied evacuees decreases to 1,733, a substantial improvement compared to the previous case. Among pedestrians, unmet demand falls from 964 to only 18, concentrated in a single sub-zone that could not be retrofitted or served by an open vertical shelter due to budget constraints. For vehicles, the number of unsatisfied passengers decreases from 4,163 to 1,715, meaning that 2,450 additional evacuees are saved. Of the unsatisfied vehicles, 768 are fully unsatisfied in 85 non-retrofitted sub-zones, 173 are partially satisfied in 11 sub-zones due to arc capacity limits, and 810 are lost because non-compliant drivers either ignore route assignments and face overcapacity or leave retrofitted sub-zones despite shelter-in-place orders and fail to reach safety within the lead time. While some of these losses are unavoidable, others stem from misassignments or suboptimal prioritization of retrofitting decisions. These may be mitigated through targeted training and awareness programs aimed at improving compliance, or by adjusting retrofit prioritization strategies.

Overall, this case demonstrates the strong effectiveness of shelter-in-place as a complementary strategy to vertical shelters. Pedestrian demand is nearly fully satisfied when budget permits, while vehicle losses are significantly reduced. Losses among vehicles primarily arise from arc capacity constraints, budget limitations that prevent retrofitting in all necessary sub-zones, and non-compliance behavior that leads to misassignments. Some losses are unavoidable, but targeted interventions can improve outcomes. The left figure shows the spatial distribution of retrofitted sub-zones and opened vertical shelters, while the right figure additionally depicts the unsatisfied evacuees in this case.

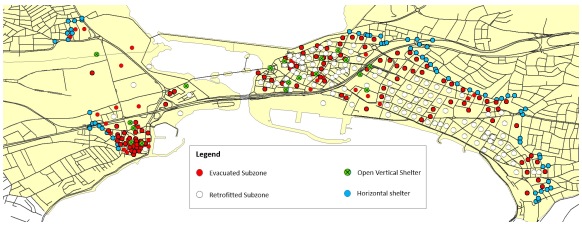

(a) Retrofitted sub-zones and opened vertical shelters in Case 3.

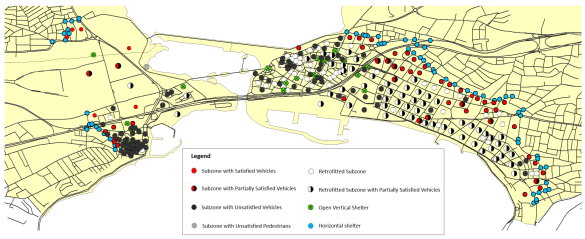

(b) Unsatisfied evacuees in Case 3.

Figure 17: Case 3 results with retrofitted sub-zones, opened vertical shelters, and unsatisfied evacuees.

5.2.4 Opening Vertical Shelter and Shelter-in-Place Considering Compliance Behavior

In the fourth case, compliance behavior is explicitly incorporated into the strategy of retrofitting buildings for shelter-in-place and opening vertical shelters. The total number of retrofitted sub-zones remains 109, although the specific sub-zones differ slightly from the previous case due to compliance-driven prioritization, while the number of open vertical shelters decreases to 17. In the left figure, we can see the distribution of the open vertical shelters and retrofitted sub-zones that reflect this adjusted prioritization.

For pedestrians, the results remain unchanged. One sub-zone lacks access to any shelter, and the budget is insufficient to retrofit its buildings or open the nearby vertical shelter. Consequently, 18 pedestrians remain unsatisfied, independent of compliance behavior.

For vehicles, the inclusion of compliance behavior improves outcomes. The number of unsatisfied passengers decreases from 1,715 in Case 3 to 1,623, a reduction of 92. This improvement arises from assigning evacuees to routes with higher compliance rates and adjusting retrofit prioritization accordingly. Among the 1,623 unsatisfied passengers, 696 reside in retrofitted sub-zones but disregard the shelter-in-place order. These losses are unavoidable within the current model, as the number of evacuees saved through retrofitting far exceeds those lost due to non-compliance. In addition to revisiting retrofit priorities, targeted awareness and training programs would be required to increase compliance in these zones. A further 57 passengers are lost because, although vehicles are directed to higher-compliance routes and arc over-capacity is avoided by incorporating non-compliant demand into capacity constraints, there are no alternative assignments for this group. Their loss cannot be prevented under the current framework, though training programs could help mitigate such non-compliance behavior. The remaining unsatisfied passengers result from capacity and time-window limitations unrelated to compliance, underscoring the need for strategies that increase effective arc capacity.

As a conclusion, the overall impact of explicitly modeling compliance behavior in this case remains limited. In general, for sub-zones without shelter access, evacuees are assumed fully compliant; as a result, the effect of non-compliance is not apparent, particularly for pedestrians, whose outcomes remain unchanged. For vehicles, incorporating compliance yields modest gains through improved routing, while shelter-in-place non-compliance remains unavoidable. Unlike route assignment, where evacuees can sometimes be directed to higher-compliance paths, no such flexibility exists for shelter-in-place, and the only possible adjustment lies in revising retrofit priorities to reduce exposure. This limited impact is partly attributable to the relatively low vehicular demand ratio, which dampens the influence of non-compliance on overall outcomes. With a higher vehicular demand ratio, however, the effect of explicitly considering compliance would become more significant, altering both retrofitting and routing priorities and

further reducing losses. The right figure additionally depicts the unsatisfied evacuees under this scenario.

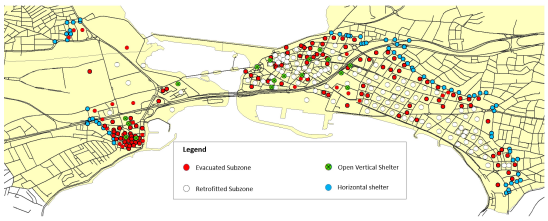

(a) Distribution of open vertical shelters and retrofitted sub-zones in Case 4.

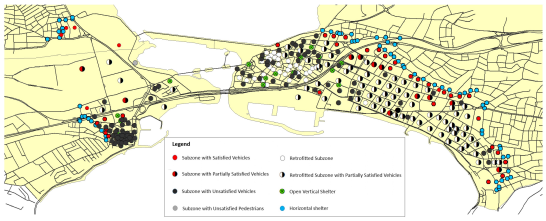

(b) Unsatisfied evacuees under compliance modeling in Case 4.

Figure 18: Results of Case 4 under compliance modeling

As noted, in many sub-zones, insufficient arc capacity leads to unsatisfied vehicles. This is most pronounced in the severely damaged area, where 86% of vehicles remain unsatisfied, as shown in Figure 19. These sub-zones were not prioritized for retrofitting because pedestrian demand dominates in this region. Most pedestrians can reach horizontal shelters without encountering capacity restrictions, while others have access to vertical shelters. Accordingly, the budget was directed to sub-zones where retrofitting yielded greater overall benefit.

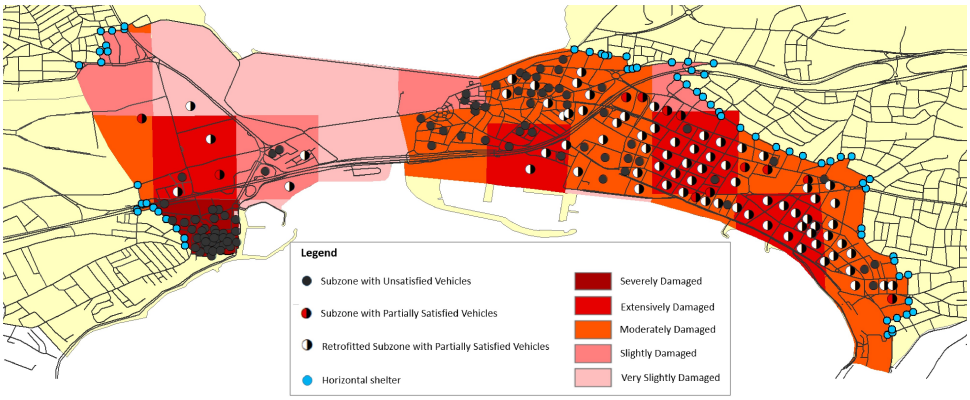

Figure 19: Severely damaged area showing high vehicle unsatisfaction due to arc capacity limits.

The next two maps illustrate compliance status under the suggested strategies and the implications for evacuees who disregard instructions and self-evacuate according to their own perceptions.

For pedestrians, only one sub-zone (marked with grey circles) cannot be assigned to any shelter and thus remains unsatisfied. In retrofitted sub-zones, full compliance is observed, while in 28 sub-zones (approximately 5% of the pedestrian population) partial non-compliance occurs. Although all non-compliant pedestrians still reach shelter due to the absence of arc capacity limits, their deviation from the prescribed plan increases exposure to tsunami inundation risk.

For vehicles, non-compliance has more severe consequences. It manifests in two forms: ignoring shelter-in-place orders and disregarding suggested routes. Unlike pedestrians, these behaviors can directly result in fatalities because vehicles are subject to strict arc capacity constraints. In this case, 758 passengers are non-compliant with shelter-in-place, of whom nearly 700 fail to reach safety, while 96 passengers are non-compliant with suggested routes,

resulting in 56 additional losses. These outcomes emphasize that, particularly for vehicles, adherence to evacuation instructions is critical for survival.

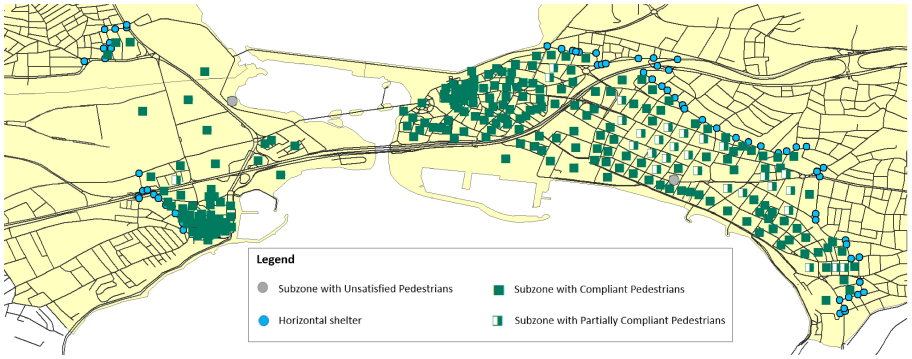

Figure 20: Compliance status of pedestrians under the suggested strategies.

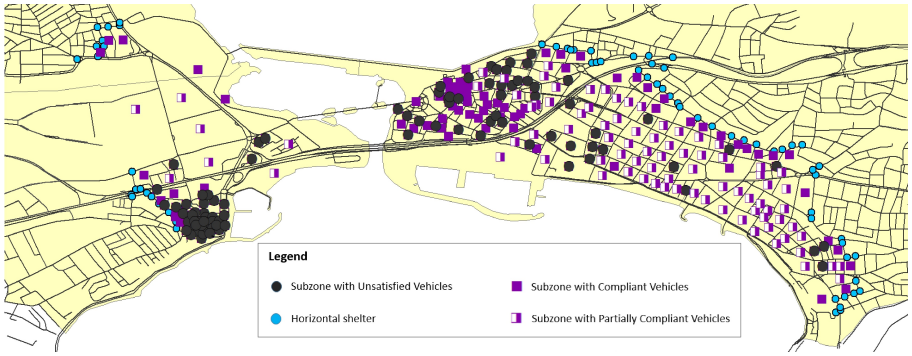

Figure 21: Compliance status of vehicles under the suggested strategies.

In the base case, congestion levels across 460 intersections were also evaluated. Approximately 1.5% of these nodes—equivalent to seven intersections—exhibited congestion due to limited arc capacities. These congested intersections generate holdover arcs in the time-expanded network, representing delays where vehicles must wait before proceeding. The relatively small number of congested nodes is partly attributable to the shelter-in-place strategy, under which a substantial portion of the population remains at home. In addition, evacuees in sub-zones without access to horizontal shelters within the available time are assumed to stay at their origin nodes until inundation, causing waiting at the origin rather than at intersections; afterward, they are assigned to a dummy node representing unsatisfied demand. Figure 22 illustrates the spatial distribution of the congested intersections, highlighted with nested circles. Addressing this issue would require targeted capacity enhancements, particularly by prioritizing the expansion of arcs connected to these critical intersections.

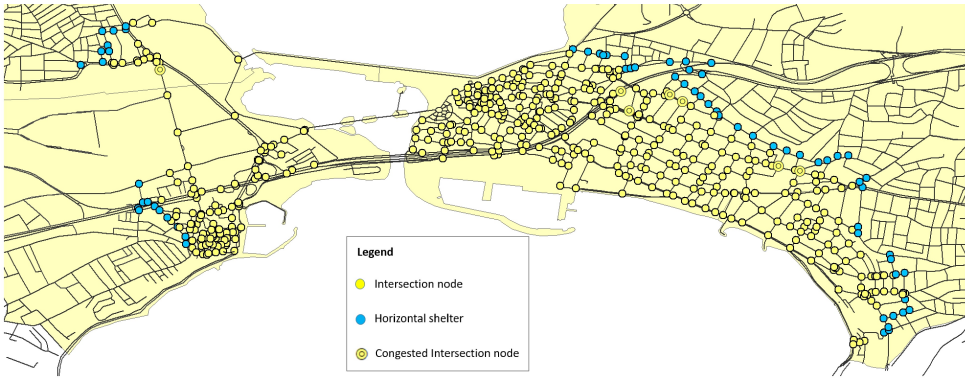

Figure 22: Congested intersections in the base case.

5.2.5 Comparison of the Four Cases

The table presents a comparative summary of all four cases. In Case 1, where no evacuation plan is implemented, the number of unsatisfied evacuees and accordingly total risk is highest. Introducing vertical shelters (Case 2) markedly reduces unsatisfied pedestrians and leads to a significant reduction in overall risk. In Case 3, combining vertical shelters with shelter-in-place through retrofitting further improves outcomes, protecting both pedestrians and vehicles and substantially lowering total risk. Nonetheless, vehicle flows continue to face arc overcapacity due to ignoring non-compliant vehicles. In Case 4, when compliance behavior is explicitly incorporated into the model, these misassignments are eliminated, congestion on critical arcs is reduced, and the numbers of both unsatisfied and non-compliant vehicles decline.

Although these strategies yield substantial improvements, further enhancements remain possible. For pedestrians, allocating additional budget to open more vertical shelters or retrofit buildings—particularly when supported by awareness and training programs to strengthen compliance with shelter-in-place—would save more lives. For vehicles, increasing retrofitting resources, together with measures that expand arc capacity or establish pre-planned evacuation corridors, would allow routing along higher-compliance paths. These strategies would mitigate non-compliance, reduce unmet demand, and further enhance the overall effectiveness of the evacuation plan.

Table 3: Comparison of outcomes across the four cases.

Strategy	Ignoring noncompliance behavior				Adjusted for Observed Noncompliance					
	Total risk	#Retrofitted zones	#open vertical shelters	Expanded capacity	Actual Risk	#Unsatisfied pedestrian	#Unsatisfied passengers	Total lost	#Congested Intersection nodes	#overcapacity arcs
No plan	18729635.9	0	0	0	18952746.5	14706	4163	18869	5	10
Vertical Shelter Opening	5034298.7	0	60	34	5257409.37	964	4163	5127	15	10
Vertical shelter and Shelter in place	956462.49	109	18	0	1781939.43	18	1715	1733	18	26
Vertical shelter and Shelter in place considering compliance behavior	1729386.5	109	17	0	1729386.5	18	1623	1641	7	0

5.3 Sensitivity Analysis

To assess the robustness of the proposed model and examine the influence of key parameters on evacuation performance, a sensitivity analysis is performed with respect to budget levels and VDR:

5.3.1 Sensitivity Analysis on Budget

In the base case where the vehicle demand ratio (VDR) is set to 16%, a sensitivity analysis was conducted to examine the impact of different budget levels on evacuation performance. As shown in Figure 23, the number of retrofitted sub-zones increases with the budget but remains nearly unchanged between four and six times the base level, indicating that while totals plateau, retrofit priorities shift to more critical sub-zones. As retrofitting expands, the number of open vertical shelters initially declines; however, at six times the base budget it rises again, reflecting a strategic shift toward additional shelter provision. This adjustment occurs because, in some sub-zones, retrofitting alone cannot save all evacuees—especially where access to horizontal shelters and non-compliance with shelter-in-place guidance limit its effectiveness—making new vertical shelters preferable when budget and capacity permit. Consequently, as the budget increases, the number of unsatisfied pedestrians and passengers declines, and total loss and overall risk decrease accordingly. Pedestrian demand is fully satisfied when the budget reaches four times the base level, whereas a fraction of vehicle users remains unsatisfied due to non-compliance and persistent capacity constraints that cannot be fully mitigated by retrofitting. Overall, the results indicate that budget expansion remarkably mitigates evacuation risk up to a threshold, beyond which strategic improvements in compliance behavior and capacity management become more influential than additional financial investment.

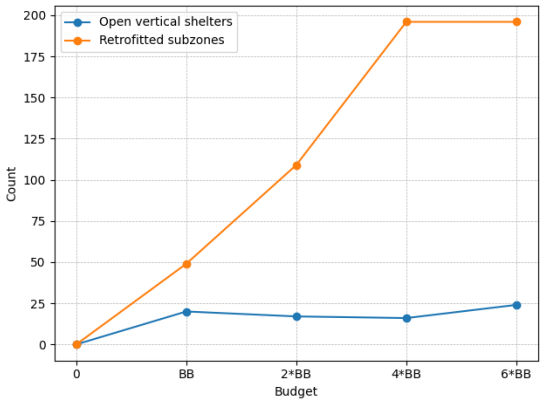

(a) Open vertical shelters & retrofitted sub-zones vs budget.

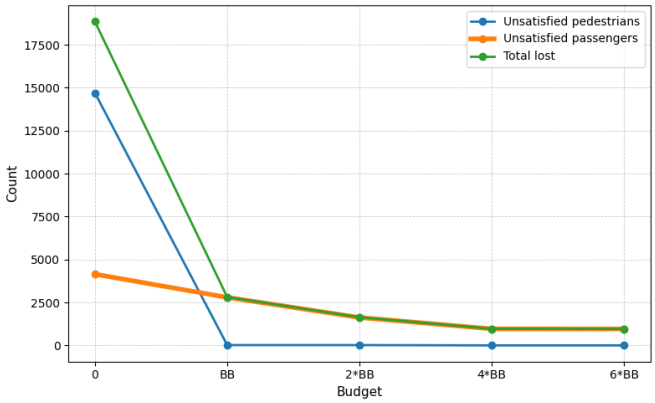

(b) Unsatisfied pedestrians, passengers, and total loss vs budget.

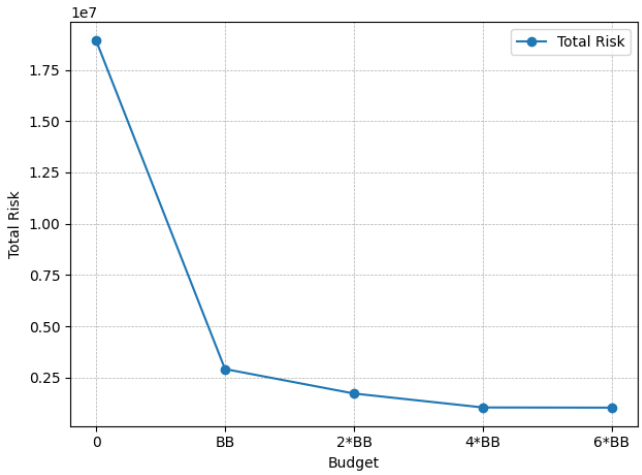

(c) Total risk vs budget.

Figure 23: Sensitivity analysis results under different Budget levels with a fixed VDR of 16%.

5.3.2 Sensitivity Analysis on VDR

When the budget is fixed at twice the base budget (as in the base case), varying the VDR influences facility utilization, evacuee satisfaction, and overall risk. As VDR increases, the number of open vertical shelters decreases because the share of pedestrians declines, reducing the need for such facilities. When all evacuees move on foot, full compliance can be achieved by opening more vertical shelters compared to retrofitting. In this case, evacuees in retrofitted subzones are not lost but contribute to overall risk due to their longer exposure, which further supports prioritizing vertical shelters. As VDR increases, the number of retrofitted subzones remains nearly constant, except for the case in which all evacuees are pedestrians. As a result, a higher VDR leads to a greater number of unsatisfied evacuees and, accordingly, higher overall risk. In contrast, when all evacuees evacuate on foot, the model can satisfy the entire demand at this budget level, indicating that this is the most effective transportation mode for tsunami evacuation. However, since it is difficult to ensure that all evacuees comply with a fully pedestrian evacuation, a mixed pedestrian–vehicle evacuation strategy should be considered.

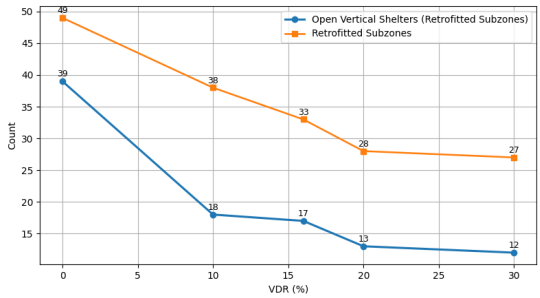

(a) Number of open vertical shelters and retrofitted subzones under different VDR levels.

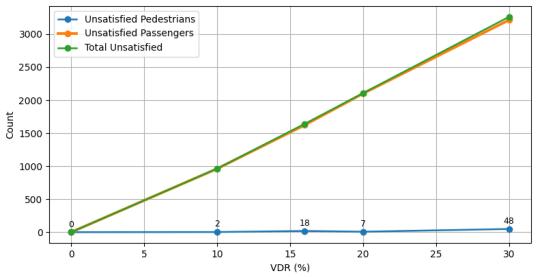

(b) Unsatisfied pedestrians, unsatisfied passengers, and total unsatisfied evacuees across VDR levels.

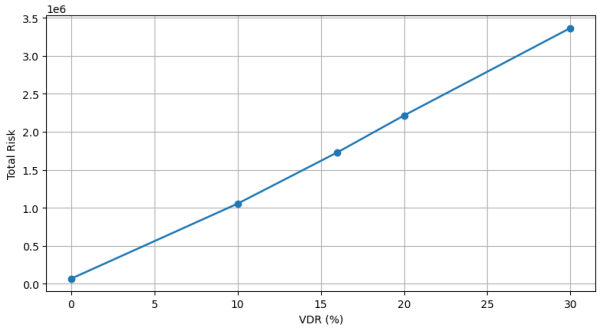

(c) Total risk under different VDR levels.

Figure 24: Sensitivity analysis results under different Vehicle Demand Ratio (VDR) levels with a fixed budget of 2×BB.

5.4 Neighborhood level analysis

Various measures for both pedestrians and vehicles are analyzed at the neighborhood level to evaluate accessibility, capacity, and demand characteristics, as presented in Figure 25. **Fatih** has the highest vehicular and pedestrian demand, a moderate average departure time, and a maximum capacity that is not particularly high. Although only about 2% of its subzones lack access to shelters, it contains the largest share of retrofitted subzones and the highest level of unsatisfied demand. This outcome reflects the combination of high demand, medium departure timing, and relatively limited capacity. **Atatürk** ranks second in demand, with an average departure time of approximately two minutes. All vehicles in this area can reach horizontal shelters before considering arc capacity; however, 71% of its subzones are retrofitted due to their low maximum arc capacity. The absence of open vertical shelters and the prevalence of medium to high damage levels across most arcs explain the need for extensive retrofitting, though the proportion of unsatisfied demand (15.8%) remains moderate. **Dizdariye**, with a demand level comparable to Atatürk, has a similar departure time and the same maximum capacity as Fatih. However, about 72% of its subzones lack vehicular access and nearly 90% lack pedestrian access, as they are located far from horizontal shelters or other safe areas. Despite hosting the highest number of candidate and open vertical shelters and retrofitting 53% of its subzones, Dizdariye still exhibits the second-highest unsatisfied demand due to persistent accessibility issues. **Mimar Sinan** ranks fourth in demand and shows the earliest average departure time, coupled with the highest maximum arc capacity. Approximately 5% of its subzones lack access before considering capacity reductions, and due to severe and high dam-

age levels along several arcs, it ranks third in unsatisfied demand. Despite this, the number of retrofitted subzones in Mimar Sinan is the fewest among all neighborhoods, likely due to its smaller population and lower retrofitting priority under budget constraints. Finally, **Ulus**, with the smallest demand, consists of only four subzones. All subzones have full access for both pedestrians and vehicles, requiring no retrofitting or vertical shelters. The entire demand in this area is successfully satisfied, and evacuees depart the latest among all neighborhoods. Overall, the results indicate that total demand, departure timing, accessibility, and the number of candidate vertical shelters jointly shape the optimal evacuation decisions across neighborhoods, emphasizing the need for capacity enhancement, public awareness to encourage earlier departures, and balanced retrofitting in highly populated areas such as Fatih and Dizdariye.

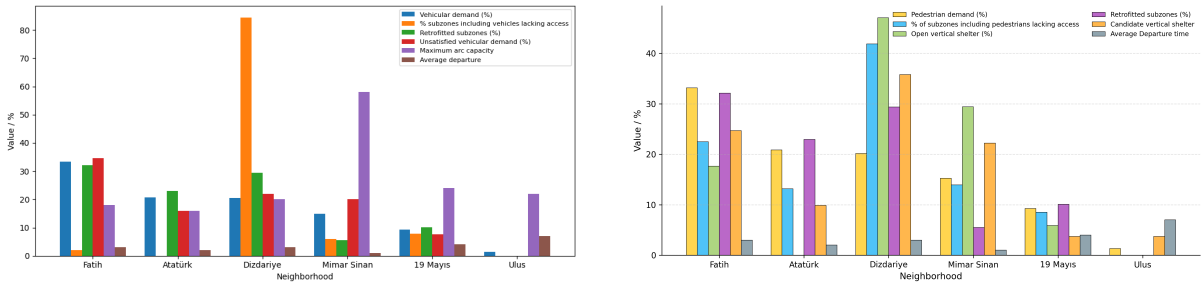

(a) Vehicular evacuation analysis by neighborhood

(b) Pedestrian evacuation analysis by neighborhood

Figure 25: Comparison of evacuation indicators across neighborhoods for vehicle (left) and pedestrian (right) scenarios.

5.5 Validation and verification of the solution algorithm and acceleration methods

The problem was solved using the suggested algorithm, and all proposed acceleration strategies were applied and proved effective in enhancing convergence and computational efficiency. Among the initial solution strategies, the third warm-start (Warm-start III) yielded the best performance. After integrating all acceleration methods—including network reduction, subproblem decomposition, MDC, and Warm-start III—the base case was solved in approximately 1,765 seconds (about 29 minutes).

6 Conclusion

This study proposed an integrated optimization framework for tsunami evacuation planning that jointly determines shelter-in-place through the retrofitting of residential buildings, the location of vertical shelters, and evacuation routing and assignment for pedestrians and vehicles under realistic behavioral and operational conditions. The model explicitly captures reduced arc capacities caused by earthquake damage, delayed departure times, and congestion effects on a time-expanded network, reflecting conditions that critically influence evacuation feasibility. Shelter-in-place is endogenized by allowing only retrofitted or engineered buildings to serve as safe refuges—an innovation not previously introduced in tsunami evacuation optimization. The framework distinguishes between pedestrian and vehicular behaviors and incorporates survey-based compliance data to represent heterogeneous decision-making. A hybrid Benders Decomposition–Column Generation algorithm is employed to solve the model efficiently, and among

the acceleration strategies tested, the use of a second initial solution set and the Maximum Density Cut provided the most substantial gains in convergence speed and computational performance. Implemented for the Büyükçekmece district of Istanbul, the model offers a realistic and behaviorally grounded foundation for optimizing evacuation and shelter decisions under severe time and resource limitations, setting the stage for several critical policy insights.

The results demonstrate that an effective tsunami response requires a carefully optimized balance between evacuation and shelter-in-place strategies, accounting for both vertical and horizontal shelters, available budgets and capacities, usable road network capacity, and evacuee compliance behavior. Assuming full compliance, retrofitting remains the preferred strategy for most zones because remaining in reinforced structures lowers exposure risk and alleviates congestion. However, limited budgets make complete retrofitting infeasible, compelling evacuation in areas farther from safe destinations or affected by late departures and capacity shortages. When non-compliance is incorporated, the evacuation strategy becomes more realistic and effective, reducing congestion and aligning outcomes more closely with actual behavior. Both non-compliant drivers and pedestrians may perceive the shortest-time routes as optimal, although congestion and arc capacity constraints render them suboptimal in practice. Consequently, in certain regions, retrofitting loses its attractiveness, and opening strategically located vertical shelters for pedestrians proves more beneficial than additional retrofitting, even at the cost of some vehicle losses. Non-compliance, while unavoidable, can be mitigated for vehicles through redistributing traffic to less congested routes, revising retrofit priorities for high-risk areas, and strengthening training and communication to improve adherence. For shelter-in-place, non-compliance remains a fixed challenge, though retrofit priorities can be adjusted to reduce exposure risk among non-compliant pedestrians. Overall, enhancing compliance, expanding critical arc capacities, and promoting earlier departures for vehicles, together with prioritizing retrofitting for pedestrians under budget constraints, lead to a significant reduction in overall risk and unsatisfied demand, yielding balanced and practically implementable evacuation strategies.

Future research can extend the present study in several directions. Incorporating uncertainty in demand and road capacity under different temporal or seasonal scenarios would enhance the model's adaptability and robustness. Moreover, considering multiple tsunami scenarios with varying risk levels and tsunami arrival times would allow for scenario-based risk assessment within the optimization framework. The current assumption that non-compliant drivers always choose the shortest-time paths can also be relaxed by considering alternative routes influenced by factors such as familiarity or congestion. To convert partially compliant evacuees into fully compliant ones, incentive-based and training-oriented strategies may be developed, such as insurance guarantees or safety certification for those sheltering in place and targeted preparedness programs for subzones with lower compliance potential or limited resources. Additionally, selectively retrofitting critical road segments in severely damaged areas and managing mixed pedestrian–vehicle interactions through dynamic traffic control could further strengthen evacuation performance.

References

Aldahlawi, R. Y., Akbari, V., and Lawson, G. (2024). A systematic review of methodologies for human behavior modelling and routing optimization in large-scale evacuation planning. *International Journal of Disaster Risk Reduction*, page 104638.

Apivatanagul, P., Davidson, R. A., and Nozick, L. K. (2012). Bi-level optimization for risk-based regional hurricane evacuation planning. *Natural hazards*, 60(2):567–588.

Arıkanoğlu, A., Moslemi, S., Bayram, V., and Yıldız, B. (2025). Modeling and simulating human behavior in large-scale emergency evacuations: A comprehensive review. Manuscript submitted for publication, SSRN preprint under review.

Bayram, V. (2016). Optimization models for large scale network evacuation planning and management: A literature review. *Surveys in Operations Research and Management Science*, 21(2):63–84.

Bayram, V., Baloch, G., Gzara, F., and Elhedhli, S. (2022). Optimal order batching in warehouse management: A data-driven robust approach. *INFORMS Journal on Optimization*, 4(3):278–303.

Bayram, V. and Yaman, H. (2024). A joint demand and supply management approach to large scale urban evacuation planning: Evacuate or shelter-in-place, staging and dynamic resource allocation. *European Journal of Operational Research*, 313(1):171–191.

Bayram, V., Yıldız, B., Doğulu, C., Yalçıner, A. C., Moslemi, S., Arıkanoğlu, A., Ergülen, , Bingöl, G. G. D., Mamouri, L., Barlas, E. A., Din, N., Ergez, D., Kulkarni, O., and Luo, M. (2025). Tsunami tehdidine karşı İstanbul İli marmara denizi kıyıları tahliye planlaması ve yönetimi araştırma projesi sonuç raporu. Technical Report Proje No: 221M165, TÜBİTAK 1001 Projesi, Ankara, Türkiye. Project Report.

Braik, A. M., Gupta, H. S., Koliou, M., and González, A. D. (2025). Multi-hazard probabilistic risk assessment and equitable multi-objective optimization of building retrofit strategies in hurricane-vulnerable communities. *Computer-Aided Civil and Infrastructure Engineering*.

Caunhye, A. M., Nie, X., and Pokharel, S. (2012). Optimization models in emergency logistics: A literature review. *Socio-economic planning sciences*, 46(1):4–13.

Cova, T. J., Dennison, P. E., and Drews, F. A. (2011). Modeling evacuate versus shelter-in-place decisions in wildfires. *Sustainability*, 3(10):1662–1687.

Dewi, R. S. (2012). A-gis based approach of an evacuation model for tsunami risk reduction. *IDRiM Journal*, 2(2):108–139.

Doerner, K. F., Gutjahr, W. J., and Nolz, P. C. (2009). Multi-criteria location planning for public facilities in tsunami-prone coastal areas. *OR spectrum*, 31:651–678.

Dogan, G. G., Pelinovsky, E., Zaytsev, A., Metin, A. D., Tarakcioglu, G. O., Yalciner, A. C., Yalciner, B., and Didenkulova, I. (2021a). Long wave generation and coastal amplification due to propagating atmospheric pressure disturbances. *Natural Hazards*, 106(2):1195–1221.

Dogan, G. G., Yalciner, A. C., Yuksel, Y., Ulutas, E., Polat, O., Guler, I., Sahin, C., Tarih, A., and Kanoglu, U. (2021b). The 30 october 2020 aegean sea tsunami: Post-event field survey along turkish coast. *Pure and Applied Geophysics*, 178(3):785–812.

Dow, K. and Cutter, S. L. (2000). Public orders and personal opinions: Household strategies for hurricane risk assessment. *Global Environmental Change Part B: Environmental Hazards*, 2(4):143–155.

Dulebenets, M. A., Pasha, J., Kavoosi, M., Abioye, O. F., Ozguven, E. E., Moses, R., Boot, W. R., and Sando, T. (2020). Multiobjective optimization model for emergency evacuation planning in geographical locations with vulnerable population groups. *Journal of Management in Engineering*, 36(2):04019043.

EM-DAT (2020a). Cred crunch 58: Disaster year in review (2019). `https://www.emdat.be/publications`. Centre for Research on the Epidemiology of Disasters (CRED).

EM-DAT (2020b). Natural disasters trends, the international disaster database. https://www.emdat.be/. Centre for Research on the Epidemiology of Disasters (CRED).

Erdurmuş, S. B. (2005). Benefit-cost analysis for retrofitting of selected residential buildings in istanbul. Master's thesis, Middle East Technical University (METU), Ankara, Türkiye. M.Sc. Thesis, Department of Civil Engineering.

FEMA (2019). Planning considerations: Evacuation and shelter-in-place. https://www.fema.gov/media-library-data/1564165488078-09ab4aac641f77fe7b7dd30bad21526b/Planning_Considerations_Evacuation_and_Shelter-in-Place.pdf. Federal Emergency Management Agency (FEMA), Washington, D.C.

FHWA (2007). Using highways for no-notice evacuations: Routes to effective evacuation planning primer series. https://ops.fhwa.dot.gov/publications/fhwahop08003/fhwahop08003.pdf. U.S. Department of Transportation, Federal Highway Administration, Office of Operations, Report No. FHWA-HOP-08-003, Washington, D.C.

Gladwin, H. and Peacock, W. (1997). Warning and evacuation: A night for hard houses. inhurricane andrew: Gender, ethnicity and the sociology of disasters, eds. bh morrow and h. gladwin, 52–74.

González-Riancho, P., Aguirre-Ayerbe, I., Aniel-Quiroga, I., Abad, S., González, M., Larreynaga, J., Gavidia, F., Gutiérrez, O., Álvarez-Gómez, J. A., and Medina, R. (2013). Tsunami evacuation modelling as a tool for risk reduction: application to the coastal area of el salvador. *Natural hazards and earth system sciences*, 13(12):3249–3270.

Gupta, H. S., Adluri, T., Sanderson, D., González, A. D., Nicholson, C. D., and Cox, D. (2024). Multi-objective optimization of mitigation strategies for buildings subject to multiple hazards. *International Journal of Disaster Risk Reduction*, 100:104125.

Hsiao, C.-C., Sun, M.-C., Chen, A. Y., and Hsu, Y.-T. (2021). Location problems for shelter-in-place deployment: A case study of vertical evacuation upon dam-break floods. *International journal of disaster risk reduction*, 57:102048.

Hu, Z.-H., Sheu, J.-B., and Xiao, L. (2014). Post-disaster evacuation and temporary resettlement considering panic and panic spread. *Transportation research part B: methodological*, 69:112–132.

Hughes, W., Zhang, W., and Ding, Z. (2022). Multiobjective optimization for hurricane retrofit to improve coastal community structural and socioeconomic resilience. *Natural Hazards Review*, 23(4):04022033.

Jenabi, M., Fatemi Ghomi, S., Torabi, S. A., and Hosseinian, S. H. (2015). Acceleration strategies of benders decomposition for the security constraints power system expansion planning. *Annals of Operations Research*, 235(1):337–369.

Jiang, Y., Xu, K., Gai, W., and Salhi, S. (2022). Emergency response for tackling major accidental toxic gas releases: What should be done and when? *Safety science*, 154:105819.

Karabuk, S. and Manzour, H. (2019). A multi-stage stochastic program for evacuation management under tornado track uncertainty. *Transportation research part E: logistics and transportation review*, 124:128–151.

Lessan, J. and Kim, A. M. (2022). Planning evacuation orders under evacuee compliance uncertainty. *Safety science*, 156:105894.

Lindell, M. K., Kang, J. E., and Prater, C. S. (2011). The logistics of household hurricane evacuation. *Natural hazards*, 58:1093–1109.

Lindell, M. K., Murray-Tuite, P., Wolshon, B., and Baker, E. J. (2018). *Large-scale evacuation: The analysis, modeling, and management of emergency relocation from hazardous areas*. CRC Press.

Lindell, M. K. and Perry, R. W. (2012). The protective action decision model: Theoretical modifications and additional evidence. *Risk Analysis: An International Journal*, 32(4):616–632.

Maly, E. and Suppasri, A. (2020). The sendai framework for disaster risk reduction at five: Lessons from the 2011 great east japan earthquake and tsunami. *International Journal of Disaster Risk Science*, 11(2):167–178.

Mawardin, A. (2018). Study on location plan of temporary shelter for tsunami disaster in kuta bay of central lombok. In *Journal of the Civil Engineering Forum*, volume 4, pages 243–252.

Moslemi, S., Bayram, V., Yildiz, B., and Dogulu, C. (2025). Survey-based statistical and predictive modeling of decision-making and compliance behavior in tsunami evacuation: The istanbul case. Unpublished manuscript.

Mostafizi, A., Wang, H., Cox, D., and Dong, S. (2019). An agent-based vertical evacuation model for a near-field tsunami: Choice behavior, logical shelter locations, and life safety. *International journal of disaster risk reduction*, 34:467–479.

Nakai, H., Horiike, R., Itatani, T., and Matsumoto, Y. (2022). Childcare center evacuation to vertical shelters in a nankai trough tsunami: Models to predict and mitigate risk. *Challenges*, 13(2):48.

Necmioglu, O., Özer Sözdinler, C., Cevdet Yalçıner, A., Heidarzadeh, M., and Ishibe, T. (2018). Challenges and requirements for near-field tsunami warning in the aegean sea and eastern mediterranean. In *EGU General Assembly Conference Abstracts*, page 12273.

Official Gazette (2023). Official gazette of the republic of türkiye. `https://www.resmigazete.gov.tr/`. Accessed February 2023.

Park, S., Van de Lindt, J. W., Gupta, R., and Cox, D. (2012). Method to determine the locations of tsunami vertical evacuation shelters. *Natural hazards*, 63:891–908.

Prater, C., Wenger, D., and Grady, K. (2000). Hurricane bret post storm assessment: A review of the utilization of hurricane evacuation studies and information dissemination. *Texas A&M Univ. Hazard Reduction & Recovery Center, College Station, Tex*.

Saharidis, G. K. and Ierapetritou, M. G. (2013). Speed-up benders decomposition using maximum density cut (mdc) generation. *Annals of Operations Research*, 210(1):101–123.

Scheer, S., Gardi, A., Guillande, R., Eftichidis, G., Varela, V., de Vanssay, B., and Colbeau-Justin, L. (2011). Handbook of tsunami evacuation planning. *Luxembourg City, Luxembourg: Publications Office of the European Union*.

Solís, D., Thomas, M., and Letson, D. (2010). An empirical evaluation of the determinants of household hurricane evacuation choice. *Journal of Development and Agricultural Economics*, 2(3):188–196.

Sorensen, J. H., Shumpert, B. L., and Vogt, B. M. (2004). Planning for protective action decision making: evacuate or shelter-in-place. *Journal of Hazardous Materials*, 109(1-3):1–11.

Sotelo-Salas, C., Monardes-Concha, C. A., Pérez-Galarce, F., and Santa González, R. (2024). A multi-objective optimization model for planning emergency shelters after a tsunami. *Socio-Economic Planning Sciences*, 93:101909.

TBMM (2021). Depreme karşı alınabilecek Önlemlerin ve depremlerin zararlarının en aza İndirilmesi İçin alınması gereken tedbirlerin belirlenmesi amacıyla kurulan meclis araştırması komisyonu raporu. https://acikerisim.tbmm.gov.tr/items/407bfd50-e570-477e-91ad-4ebf58cf9225/full. Türkiye Büyük Millet Meclisi (TBMM), Accessed: November 22, 2024.

Tufekci-Enginar, D., Dogan, G. G., Suzen, M. L., and Yalciner, A. C. (2022). Performance analysis of open-source dems in tsunami inundation modelling. *Earth Science Informatics*, 15(4):2447–2466.

TÜİK (2021). Turkish statistical institute (tÜİk) population statistics, 2021. https://data.tuik.gov.tr/. Türkiye İstatistik Kurumu (TÜİK), Accessed: November 22, 2024.

Wang, Q. and Wallace, S. W. (2022). Non-compliance in transit-based evacuation pick-up point assignments. *Socio-Economic Planning Sciences*, 82:101259.

Whitehead, J. C., Edwards, B., Van Willigen, M., Maiolo, J. R., Wilson, K., and Smith, K. T. (2000). Heading for higher ground: Factors affecting real and hypothetical hurricane evacuation behavior. *Global Environmental Change Part B: Environmental Hazards*, 2(4):133–142.

Wood, N., Jones, J., Schelling, J., and Schmidtlein, M. (2014). Tsunami vertical-evacuation planning in the us pacific northwest as a geospatial, multi-criteria decision problem. *International journal of disaster risk reduction*, 9:68–83.

Wu, H.-C., Lindell, M. K., and Prater, C. S. (2012). Logistics of hurricane evacuation in hurricanes katrina and rita. *Transportation research part F: traffic psychology and behaviour*, 15(4):445–461.

Yi, W., Nozick, L., Davidson, R., Blanton, B., and Colle, B. (2017). Optimization of the issuance of evacuation orders under evolving hurricane conditions. *Transportation Research Part B: Methodological*, 95:285–304.

Yıldırım, Ş. and Yıldız, B. (2021). Electric bus fleet composition and scheduling. *Transportation Research Part C: Emerging Technologies*, 129:103197.

İBB (2023). Istanbul province possible earthquake loss estimates update project. Technical report, Istanbul, Turkey. Available at: https://depremzemin.ibb.istanbul/.

İBB-ODTÜ (2018). İstanbul İli marmara kıyıları tsunami modelleme, hasar görebilirlik ve tehlike analizi güncelleme projesi. https://depremzemin.ibb.istanbul/en/istanbul-province-marmara-coast-tsunami-modeling-vulnerability-and-hazard-anal İstanbul Büyükşehir Belediyesi (İBB) – Orta Doğu Teknik Üniversitesi (ODTÜ), Accessed: November 22, 2024.

İBB-ODTÜ (2019). İstanbul İli tsunami eylem planı. https://depremzemin.ibb.istanbul/en/wp-content/uploads/2020/07/AVCILAR_TSUNAMI.pdf. İstanbul Büyükşehir Belediyesi (İBB) – Orta Doğu Teknik Üniversitesi (ODTÜ), Accessed: November 22, 2024.